Journal of Applied Physics

Volume No. 12

Issue No. 1

January - April 2024

ENRICHED PUBLICATIONS PVT. LTD

S-9, IInd FLOOR, MLU POCKET,
MANISH ABHINAV PLAZA-II, ABOVE FEDERAL BANK,
PLOT NO-5, SECTOR-5, DWARKA, NEW DELHI, INDIA-110075,
PHONE: - + (91)-(11)-47026006

Journal of Applied Physics

Aims and Scope

The Journal of Applied Physics is published quarterly by Enriched publications. Journal of Applied Physics is peer reviewed journal and monitored by a team of reputed editorial board members. This journal consists of research articles, reviews, and case studies on Science Technology. This journal mainly focuses on the latest and most common subjects of its domain.

Journal of Applied Physics

Journal of Applied Physics

(Volume No. 12, Issue No. 1, January - April 2024)

Contents

Storage Stability of Biodiesel: A Review

Ashok Kumar Yadav[1‡], M. Emran Khan [2], Amit Pal[3], AlokManas Dubey[4]
[1]Assistant Professor,Department of Mechanical Engineering,
Raj Kumar Goel Institute of Technology,
Ghaziabad, 201003, India
ashokme015@gmail.com
[2]Professor, Department of Mechanical Engineering,Faculty of Engineering & Technology,
Jamia Millia Islamia, New Delhi – 110025, India
Email: mikhan@jmi.ac.in
[3]Associate Professor, Department of Mechanical Engineering,
Delhi Technological University,
Delhi 110042, India
Email: amitpal@dce.ac.in
[4]Professor,Department of Mechanical Engineering,
Raj Kumar Goel Institute of Technology, Ghaziabad, 201003, India
Email:alokmanas28@rediffmail.com
[‡]Corresponding author ;Tel: 8285423046

A B S T R A C T

Global warming, a spurt in population growth and an increase in demand for transport fuels in developing economies, all coupled together with limited reserves of fossil fuels, are realities that have convinced many countries of the need to develop alternative and renewable energy sources such as biofuels. Biodiesel is considered to be apromising alternative biofuel. Recently, biodiesel has received additional attention and intense research has been performed in this field all over the world due to its lower environmental impact compared to the conventional diesel fuels.The main problem of using biodiesel as fuel is its poor stability characteristics. Poor stability leads to gum formation which further leads to a storage problem of these fuels for a longer period of time. Oxidative degradation occurs in biodiesel on aerobic contact during storage as well as with metal contaminants. Antioxidants are very effective for the eradication of those oxidation stability problems. This article presents an overview of the factors affecting the oxidation stability of biodiesel and the methods available for the prediction of oxidation stability.The effect of antioxidants in preventing the oxidation of biodiesel is also discussed.

Keywords—Biodiesel; Oxidative stability; Stability parameters; Antioxidants

1 INTRODUCTION

Stability is one of the important criteria concerning fuel properties. The stability of biodiesel is lower than common diesel fuel. The formation of deposits and gum and the darkening of fuels as a result of the formation of contaminants, such as alcohols,acids, aldehydes, peroxides, etc., occur during long-term storage of biodiesel fuel [1-2]. Various processes, including oxidation in aerobic conditions, hydrolysis

in the presence of moisture, thermal decomposition by excess heat, contamination of impurities, etc., account for the instability of biodiesel that can change the fuel properties considerably [4-5]. Among these processes, oxidation is one of the significant stability concerns associated with bio diesel because it has a lower resistance capacity to oxidation and can easily be affected by air oxidation during long-term storage [3]. The composition of the fatty acid portion of the biodiesel ester molecule is the most important factor that affects its properties. The composition varies based on the feedstock used for biodiesel production. When compared to diesel fuel, the unsaturation in the molecule accounts for biodiesel instability. As the unsaturation in the fatty acid chain portion increases, the biodiesel becomes more unstable. Oxidation starts at the allylic positions to double bonds. Therefore, the fatty acid composition of the ester, especially the position of and the number of allylic and bis-allylic methylene moieties adjacent to the double bond, determines the rate of oxidation. In Fig. 1, the positions in the oleic acid, linoleic acid and linolenic acid (most common unsaturated acids present in the oils or fats and thus in the biodiesel) that are vulnerable to oxidation are highlighted by a circle with dotted lines. The allylic and bis-allylic methylene moieties are the most susceptible to oxidation as a result of the radical chain reaction [3].The oxidative degradation during long-term storage occurs mainly in the presence of air, heat, light and pro-oxidants [1-3]. Biodiesel oxidation is of two typesauto-oxidation and photo-oxidation. Auto-oxidation is a major cause of biodiesel oxidation. The auto-oxidative degradation of biodiesel is a radical chain reaction and involves initiation, propagation, and termination steps. During the initial stages of biodiesel oxidation, the methylene groups allylic and bis-allylic to the double bonds are more active and hydrogen radicals are abstracted by radical initiatorsThe resultant radicals interact with oxygen, which results in peroxide formation for the propagation step. The peroxides propagate the chain reaction by the further abstraction of hydro- gen from the methylene moieties and form carbon radicals and hydro peroxides. Next, the newly formed carbon free radicals will again combine with oxygen and continue the propagation process. This chain process continues until the termination step, which provides the formation of stable products the hydro peroxide formation during the auto-oxidative degradation of linoleic acid methyl ester. The ultimate decomposition of peroxides results in the formation of aldehydes, such as hexenals [1,18]. At high temperatures, highly stable conjugated structures are formed by the isomerization of methylene-interrupted polyunsaturated olefin units. For the isomerisation process, one of the conjugated diene groups in the chain can react with the olefinic group from the nearby fatty acid chain and can form a substituted cyclohexene ring from the Diels alder reaction. At high temperatures of 180 0C, thermal dimerization occurs for the fatty acid methyl ester due to the Diels Alder reaction and forms the dimer. shows the cyclohexene ring formed from linoleic acid methyl ester and illustrates the formation of dimers via the Diesel Alder reaction of linoleic acid methyl esters. The same reactions can also occur during the frying process of oil or fat and can adversely affect the performance of biodiesel obtained from used cooking oil or animal fat. The fatty acid compositions (mass%) of several biodiesel feed- stocks are given among the different feedstock shown in, coconut oil

has a small amount of unsaturated fatty acid (9%) and may be less susceptible to oxidation. Additionally, feedstock with more unsaturated fatty acid part may have more bis-allylic hydrogen and may generate less stable biodiesel. Among the different feedstock given in the table, linseed oil (with 53% linolenic acid) may have the highest tendency for oxidation based on its fatty acid composition. Most of the parameters affecting the oxidation stability also depend on the fatty acid composition of the ester.

2.PARAMETERS INDICATING THE EXTENT OF OXIDATION STABILITY OF BIODIESEL

An understanding of selected fuel parameters is highly important in evaluating the oxidation stability of biodiesel. Most of those parameters are directly related to the fatty acid composition of the biodiesel ester molecules. The important parameters that help to predict the oxidation stability of a biodiesel sample, their determination and its effect on the oxidation of biodiesel are discussed below.

2.1 Iodine value (IV)

The estimation of the IV for biodiesel fuel, which is the measure of the total degree of unsaturation, provides useful guidance for preventing various problems in engines. The IV is based on the reactivity of alkyl double bonds, and an increased IV of biodiesel indicates the possibility for the formation of various degradation products that can negatively affect engine operability and reduces the quality of lubrication [1]. The IV is expressed as the gram of iodine consumed per 100 g of the substance, which is the most parameter employed for determining the magnitude of unsaturation in the esters of fatty acids, fats, oils and their derivatives [1-4]. The local and international standard organisations provided procedures for the determination of IV in biodiesel.The IV indicates the tendency of biodiesel to oxidise or polymerise, which leads to the formation of insoluble sediments. An increase in the degree of unsaturation causes an increase in the iodine used. The IV considers that the nature, position in the chain and the amount of oleniccarbons in the fatty compounds are equal and thus equally reactive, which makes the IV not able to distinguish the structural differences that are present in different fatty compounds [3]. Therefore, the IV does not provide a measure to determine whether the hydrogens are allylic or bis-allylic to the double bonds, which is an important factor for determining the oxidisability of biodiesel. Biodiesel stability is not related to the total number of double bonds expressed by the IV but is mainly related to the number and position of the bis-allylic methylene moieties adjacent to the double bond.

2.2 Induction period (IP)

Biodiesel oxidation is mainly the result of a radical chain reaction that causes the formation of hydro peroxides. During the initial period of storage, the formation of hydro per- oxides is very low. This dead

. This characteristic time period is called the induction period (IP). The relative oxidation rate study of the methyl esters conformed that biodiesel with more poly-un-saturations in the sample can easily experience oxidation [5]. The oxidation rate of oleic (18:1), linoleic (18:2), and linolenic (18:3) acids is noted as 1:12:25. Additionally, the stability predicting parameter, called the oxidation stability index, is related to the IP. The minimum IP limits, which are specified by the American (ASTM D6751-11b) [1] and European (EN 14214) [26] standards for biodiesel in the resistance of oxidation, are 3 h and 6 h, respectively. The Indian speciation IS-15607 recommends a minimum of 6 h as the induction time.

2.3 Peroxide value (PV)

The PV is generally based on the primary oxidation products, such as the hydro peroxides of the biodiesel, and is a measure of the peroxide units formed during the oxidation process. The PV is measured in mill equivalents of peroxide units per kg of the biodiesel sample. The PV influences various parameters in the fuel standard, such as the cetane number (CN), density, viscosity, etc. [13]. The increase in PV increases CN, which may reduce the ignition delay time [12]. The increase in PV as well as the acidity after the IP can also cause the corrosion of the fuel system components, the hardening of the rubber components, the fusion of the moving components and engine operation problems Several studies exist for storage stability tests for biodiesel, which show that oxidation can affect fuel quality with respect to the PV [15] report that a low PV is required for the high stability of biodiesel against oxidation. [1] haveanalyzed the PV of karanja oil methyl ester (KOME). According to the results obtained from the 180-day storage study, the PV increased as the storage time of biodiesel increased. Therefore, oxidation stability decreases with an increase in storage time.

2.4 Viscosity

Lower atomization characteristics in the fuel injector are the result of higher viscosity and create many severe effects on engine performance [7-8].The blending of biodiesel is an effective method for improving the properties at low temperatures [9-12].Because the vaporization and atomization of the fuel is reduced as a result of the high viscosity of the fuel, the fuel requires the viscosity of biodiesel increases with an increase in the carbon chain length, the degree of saturation of the fatty acid and its ester and the presence of free fatty acids. The viscosity of the biodiesel obtained from the used cooking oil is higher than the biodiesel obtained from neat vegetable oils. Samples with cis double bond configurations have lower viscosity, whereas samples with trans double bonds have higher viscosity. However, the position of the double bond has a minor effect on the viscosity .Highly viscous samples also have a high tendency for oxidation. The main reason for the rapid oxidation processes with a high viscosity is due to the isomerization of the double bond, usually cis to trans, along with the formation of high molecular weight products. Viscosity is useful for the measurement of the oxidation progression of biodiesel. The polymeric secondary oxidation products of biodiesel cause the formation of soluble gums

and insoluble sediments and will result in an increase in the viscosity.

3.METHODS USED TO PREDICT THE STABILITY OF BIODIESEL

A wide variety of techniques have been used for the stability determination of fatty acid esters. The type of test method depends mainly upon the nature of the stability, including thermal stability, oxidation stability and storage stability. For the determination of thermal stability, the Rancimat test, ASTM D6408-08 and TGA/DTA are used. For the storage stability determination, a modified Rancimat test, ASTM D4625-04, and ASTM D5304-06 are used. The Active Oxygen Method (AOM), ASTM D2274, ASTM D3241, EN 14112, and ASTM D5483 are the methods used for the oxidation stability determination of biodiesel.

3.1 ASTM D4625-04

The ASTM D4625-04 method is the most widely established method for the estimation of storage stability for the middle distillate petroleum fuels [1]. In this method, the fuel is stored at a temperature of 43 1C for a period of time, such as 24 weeks. The sample is then filtered to evaluate the insoluble sediments of the sample, and the remaining filtrate was investigated to deter- mine the total AV and kinematic viscosity. These tests must be carried out weekly. For the precipitation of polar polymers present in the sample, isooctane is added. This modification is necessary in cases where soluble products are formed by the oxidation [1-3]. Because the temperature in the test conditions is slightly higher than room temperature, fuel oxidation and other degradative reactions lead to the formation of sediment that is mildly accelerated in this method when compared with typical storage conditions. In this method, the storage stability prediction is more reliable than the other more accelerated tests. However, because the storage periods are lengthy (4–24 weeks), the test method is not appropriate for quality control testing and only provides a tool for research on the storage properties of fuels. The storage material is also an important aspect for this study.

3.2 ASTM D6468-08 – light reflectance method

For the high temperature stability determination of the middle distillate fuels (including biodiesel), the ASTM D6468-08 method is more prominent [1]. Here, the sample is aged at 150C in open tubes with air contact for approximately 90 or 180 min. After the aging process, the sample is cooled and the insoluble sediments are filtered and estimated by the light reflectance method of the filter paper. For comparison purposes, a blank is conducted without the sample using an unused filterpad [6]. The filter paper used for this ASTM method has a nominal porosity of 11 μm, and thus, it cannot capture all of the sediment formed during aging, although it allows differentiation over a broad range of particle sizes for the sediments. The method of reflectance measurements can be affected by the colour of the filterable

insoluble and may thus not be successfully correlated to the mass of the material that is filtered. Thus, the accuracy of the method is not 100%. This method can provide an estimate of the stability of fuel when exposed to high temperatures in situations, including a recirculating engine or burner fuel delivery system, and under other high temperature conditions with limited exposure to air. In addition, the test method is also helpful in the study of operational problems related to fuel thermal stability. This method is not suitable for fuels whose flash point is less than 38 1C. This test method is also not suitable for fuels containing residual oil and is thus only suitable in the estimation of the high temperature stability of biodiesel with a very high FAME content.

3.3 ASTM D2274 – gravimetric analysis

This method is based on the filtration, which is followed by the gravimetric analysis of the insoluble materials that are formed by the oxidation in the presence of heat. Here, the sample is first aged at 95 C for 16 h by the bubbling of oxygen at a rate of 3 L/h. The insoluble sediments formed by the thermal oxidation stick on the oxidation cell and are detached with the help of a tri-solvent containing equal parts of toluene, acetone, and methanol. The solvent is then evaporated to recover the insoluble sediments (insoluble) formed. The total yield of the insoluble, expressed as milligrams per 100 ml, is reported as total insoluble. An additional analysis exists for the determination of biodiesel-soluble polymers. In this case, iso-octane is added to the sample so that the soluble polymers will precipitate. This precipitate is filtered to acquire the measure of the soluble polymers [1,3]. The use of an elevated temperature and a pure oxygen atmosphere for the test may cause differences in the nature and amount of insoluble formed in real storage situations. This test method is also not applicable to fuels containing residual oil. This test method has not been validated for the testing of biodiesel or blends of middle distillates and biodiesel meeting ASTM specifications. The test method D7462 is more suitable for testing B100 and all blends of middle distillates and biodiesel because samples containing biodiesel can cause a partial dissolution or compromise of the membrane filter, providing erroneous results.

3.4. EN 14112, Rancimat method-IP measurement

The Rancimat method is the usual and the official method for determining the oxidative stability of oils and fats by the American Oil Chemists' Society (AOCS). In this method, the temperature range is usually limited to a maximum of 130 C [1]. After that, air is bubbled through the sample so that the oxidation of the sample takes place. As a result of the oxidation process, a release of some gases along with the air occurs, which is then passed to deionized water in a flask. Theflask has an electrode, which is connected to a device for a measurement of the conductivity. The induction period (IP) is measured for this test method. Here, the IP is noted as the time at which the conductivity starts to increase very quickly. The continuous measurement of this conductivity gives an oxidation curve. The point of inflection of this curve is known as the induction period. Volatile acidic gases, such as formic acid, acetic

other acids, are produced by the oxidation and are absorbed in the water, which is the main reason for the increment in the conductivity and in the IP measurement [1,3].

3.5 Effect of antioxidants on the biodiesel stability

It is evident from literature that higher concentration of antioxidants is more effective in radical trapping and hence minimize the extent of oxidation of a biodiesel. The increase in viscosity of the biodiesel sample over a period of time is an indicator of loss of stability i.e. this value provides an indication of the oxidative reactivity of a biodiesel. Both synthetic and natural antioxidants showed that they were able to retard the oxidation process and improve the storage stability.However, the synthetic antioxidant (BHT) showed better performance when compared to natural antioxidant. These results have clearly showed that the type of antioxidant and its dosage plays an important role in retarding auto oxidation of biodiesel during storage. The results of these experiments (acid value vs. time and viscosity vs. time) contributed to the development of a predictive model.[3]

3.5 Effect of metal contaminants and the storage container on the stability of biodiesel

The presence of metal contaminants is another reason for the deterioration of biodiesel during storage. Eduardo Pereyra mentioned about the storage materials for biodiesel [3]. Biodiesel undergoes an interaction with the metals, especially with Cu and its alloys, and as a result, insoluble sediments are formed in bulk quantities by the oxidation process. Among the different metals, Cu has the strongest catalyzing effect on the oxidation process. In addition, biodiesel is infused into plastic materials, such as ethyleneand polypropylene, during its contact [1,3]. Therefore, these plastic materials and Cu-containing tanks are not suitable for the storage of biodiesel. In the case of metals and alloys, the compatible ones include aluminium, carbon steel, stainless steel and fibre glass [26]. Storage materials made up of copper, bronze, tin, zinc, etc. may hasten the oxidation of biodiesel and may result in the formation of insoluble sediments.

4. CONCLUSIONS

The biodiesel stabilitymay be affected by large number of parameters which can be categorized by oxidation, thermal and storage stability parameters. The present review has covered the different types of the fuel stabilities, mechanism of occurrence and correlations/equations developed to investigate the impact of various stability parameters on the stability of the fuel. Main parameters related to stability are PV, AV, IP, BAPE, APE, OSI and OX. And it was found that impact of APE is more on induction period than with that of BAPE. A review of the use of different types of natural and synthetic antioxidants has also been presented which indicates that natural antioxidants, being very sensitive to biodiesel production techniques and the distillation processes have varying impacts on the fuel stability. The work

on the use of synthetic antioxidants on the stability of biodiesel fromvarious resources have indicated that out of various synthetic antioxidants studied so far only 3 antioxidants have been found to increase the fuel stability significantly. However, effectiveness of these antioxidants is if the order of TBHQ > PY >PG. The reviewreveals that, lot ofworkis requiredtobe done for stability of non-edible oils. Apart from this, additional research is required to be done to investigate the effect of stability of biodiesel on engineperformance as well as effect on emissions.

REFERENCES

[1] ZahiraYaakob, Binitha N. Narayanan , SilijaPadikkaparambil , Surya Unni K. , Mohammed Akbar P.A review on the oxidation stability of biodiesel,Renewable and Sustainable Energy Reviews(2014)

[2] Siddharth Jain, M.P. Sharma, Study of oxidation stability of Jatropha curcas biodiesel/ diesel blends, energy and environment

[3] A. VenkatramKiran, J. Jayapriya&. Manoj Ravi (2015): Evaluation and Predictive Model Development of Oxidative Stability of Biodiesel on Storage, Chemical Engineering Communications, DOI: 10.1080/00986445.2015.1085383

[4] M. Balat and H. Balat, "Progress in biodiesel processing," Appl. Energy, vol. 87, pp. 1815-1835, 6, 2010.

[5] A. Pal, A. Verma, S S. Kachhwaha, S. Maji, Biodiesel production through hydrodynamic cavitation and performance testing. Renewable Energy, 35, 619(2010).

[6] Raheman, H., Phadatare, A.G. Diesel engine emissions and performance from blends of karanja methyl ester and diesel. Biomass Bioenergy, 27, 393–397, (2004).

[7] Shahidi F, Zhong Y. Lipid oxidation and improving the oxidative stability. ChemSoc Rev 2010;39:4067-79.

[8] Yadav, A.K..Khan, M.E. Dubey, A. M. Pal, A. Performance and emission characteristics of a transportation diesel engine operated with non-edible vegetable oils biodiesel, Case Studiesin Thermal Engineering 8(2016)236–244

[9] Monyem A, Van Gerpen JH. The effect of biodiesel oxidation on engine

[10] A.K. Yadav et al., Kaner biodiesel production through hybrid reactor and its performance testing on a CI engine at different compression ratios, Egypt. J. Petrol. (2016), http://dx.doi.org/10.1016/j.ejpe.2016.07.006

[11] Ryu K. The characteristics of performance and exhaust emissions of a diesel engine using a biodiesel with antioxidants. Bioresource Tech. 2010; 101: 578–582.

[12] Yadav, A.K., Khan, M.E., Pal, A., Sharma, D. Optimisation of biodiesel production from bitter groundnut oil using Taguchi method and its performance and emissions characteristics on a 4-cylinder Tata Indica engine', Int. J. Sustainable Agricultural Management and Informatics, Vol. 1, No. 4, pp.285–300,2015

[13] Rao TV, G. Rao P, K. Reddy HC. Experimental investigation of 458 Pongamia, Jatropha and Neem methyl esters as biodiesel on c.i. engine. Jordan J Mech. and Ind. Eng. 2008;460 2(2):117 –22

[14] ChakrabortyM, BaruahDC. Investigationofoxidationstabilityof Terminaliabelericabiodiesel anditsblendswithpetrodiesel.FuelProcessTechnol 2012;98:51–8.

[15] Hiroaki Imahara, Eiji Minami, ShusakuHari, SakaShiro. Thermal stability of biodiesel in supercritical methanol. Fuel 2008;87(1):1–6.

[16] BannisterCD, ChuckCJ, BoundsM, HawleyJG. Oxidativestabilityofbiodiesel fuel. ProcInstMechEngPartD:JAutomobEng2011;225:99–114.

[17] Santos NA, Cordeiro AMTM, Damasceno SS, Aguiar RT, Rosenhaim R, Filho JRC, et al. Commercial antioxidants and thermal stability evaluations. Fuel 2012;97:638-43.

[18] Xue, J., Grift, T.E.; Hansen, A.C. Effect of biodiesel on engine performances and emissions. Renew. Sustain. Energy Rev., 15, 1098–1116. (2011)

Structure Of Liquid And Comparison Of Adhesive Force With Cohesion Force

J.Nirmala[1]
[1]Assistant professor, Department of Mathematics,
KG College of Arts and Science, Coimbatore, Tamil Nadu, India.

A B S T R A C T

This paper shows the structure of a liquid based on the degrees of freedom that the molecules have for motion is determined by the number of coordinates that are occupied by cohesion. It gives the structure of liquid- surface model, string model and ring model. Various important properties of cohesion and adhesive forces are also discussed briefly. Also cohesion force is compared with adhesive force and the results are tabulated in this paper.

INTRODUCTION

We know that the structure of matter depends upon degrees of freedom for free molecular motion. Molecules in the solid state do not have the degrees of freedom for free molecular motion, while in the liquid state, the molecules have two coordinates of free space for molecular motion and the molecules in the gas phase have three coordinates of free space for molecular motion. This paper will examine cohesion as fundamental force and show the structure of liquid. Fluid dynamics is a sub discipline of fluid mechanics that deals with fluid flow-the natural science of fluids (liquids and gases) in motion. It has several sub disciplines in itself, including aerodynamics (the study of air and other gases in motion) and hydrodynamics (the study of liquids in motion). Fluid dynamics has a wide range of applications, including calculating the forces and moments on the aircraft and also determining the mass flow rate of petroleum through the pipelines, predicting weather patterns, understanding nebulae in interstellar space and modelling fission weapon detonation. The solution to a fluid dynamics problem typically involves calculating various properties of the fluid, such

as velocity, pressure, density, and temperature, as functions of space and time.

Before the twentieth century, hydrodynamics was synonymous with fluid dynamics. This is still reflected in names of some fluid dynamics topics, like magneto hydrodynamics and hydrodynamic stability, both of which can also be applied to gases.

A common characteristic of all fluids, whether Newtonian or not, is that they do not slip at a solid boundary. No matter how fast they flow away from the boundary, fluid particles at a solid surface become entrapped by the surface structure. The macroscopic effect is that the fluid velocity equals the solid velocity at a boundary. This is called the no-slip condition where the solid is fixed, so that the fluid velocity drops to zero there. No-slip sets up a slow-moving shear layer or boundary layer when fluid flows near a solid surface. The theory of boundary-layer flow is well developed and explains many effects involving viscous flow past immersed bodies or within passages.

A matter is based on its physical and chemical structure which is made up of atoms and molecules. Molecules as components of matter are common in organic substances. Solid is one of the others existing in liquid, gas and plasma. It is characterized by structural rigidity and

resistance to change of shape or volume. Unlike a liquid, a solid object does not flow to take the shape of the container, nor does it expand to fill the entire volume available to it like a gas does. Force is the external agency applied on a body to change its state of rest and motion. Pressure is the amount of force acting per unit area. A surface is two dimensional which means that at each point there is a coordinating patch on which a two dimensional coordinate system is defined.

If molecule is in liquid state, it has two coordinates of free space for molecular motion, in solid phase do not have degrees of freedom for molecular motion and in gas state it has three coordinates for free molecular motion. In this article we conclude that the cohesion is considered to be fundamental force and also the structure of liquid- surface model, string model and ring model.

VISCOUS AND INVISCID FLOW

Suppose that the fluid element is enclosed by the surface S. Let ds be the surface element around a point P. Then asurface force acting on the surface may be resolved into normal direction and tangential direction. Normal forces per unit area is said to be normal stress (pressure). The tangential forces per unit area is called shearing stress.

A fluid is said to be viscous (real fluid) when normal stress as well as shearing stress exists.A fluid is said to be inviscid (ideal fluid), if there is no friction and no tangential or shearing stress eg: oil- viscous fluid, dam water- inviscid fluid.

Existence of Normal and Shearing stresses

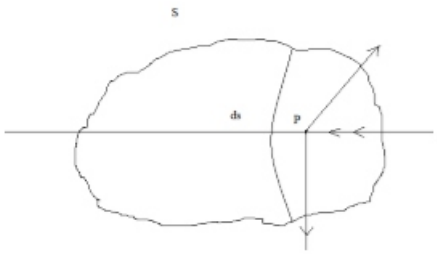

COHESION FORCE

Cohesion or cohesive force is the action in which the molecular force acts between the particles within a body or substances to unite them. In other words, cohesion allows for surface tension that creates a solid like state upon which low density materials can be placed.

Let us consider cohesion in water; it has the properties of water molecules that make them stick together. For an example take a teaspoon of water, it has more than fifty drops of water. There we can find one millions of water molecules in each drop of water. There are one atom of oxygen and two atoms of hydrogen in a molecule of water. We know that, H2O is the molecular formula of water. Here the oxygen and hydrogen both are fixed tightly together by bonds.

Condensation force present between the molecules is mentioned above. Now we define that cohesion and condensation force are one and the same.The gas state have no coordinates, and there is one coordinate space occupied by liquid state and three coordinates spaces by solid state, since cohesion is considered to be fundamental force.

Cohesion force and the size of molecules are proportional to each other. In liquid state or in solid state of matter, the intermolecular distance depends upon the size of molecules. The molecules are brought together by cohesion force, but by the action of natural force of the repulsive electromagnetic effect between the pair of electrons, the molecules wag about equilibrium state. Electro-magnetic force is the force between charged particles such as the force between two electrons. It is attractive for unlike charges and repulsive for like charges.

Forces existing between molecules

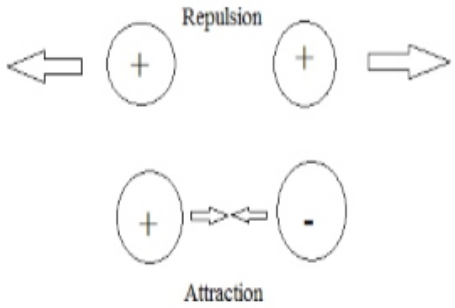

Molecules are wag under the influence of cohesion causes electro-magnetic repulsion and attraction of molecules.

STRUCTURE OF LIQUID

Let us define the structure of the liquid by using a diagram.

Molecule in liquid state

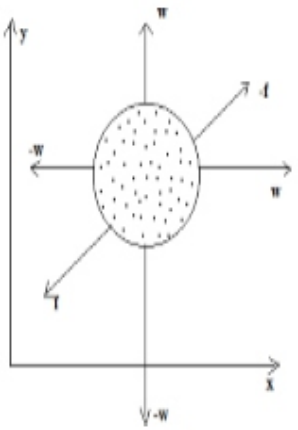

It represents a molecule in the liquid state. There are two coordinates for the motion and one coordinate is taken by cohesion. These arrangements of molecules in the space have the possibilities of developing three models for a liquid. They are surface model, ring model and string model.

SURFACE MODEL OF LIQUID

It is formed on the basis of hypothesis that translation is only made up of molecular motion. On this type, molecules are in free motion on the surface. The cohesion force is displaced. Thus, the force does not act between two molecules but somewhat between two surfaces.

Diagrammatic representation of surface model

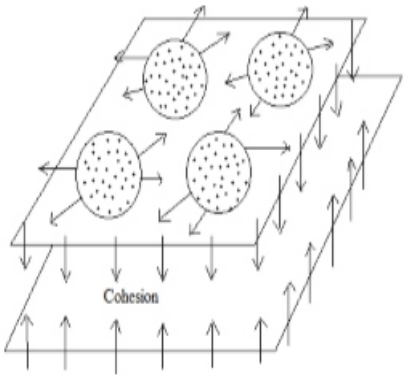

THREE SURFACE MODEL OF LIQUID

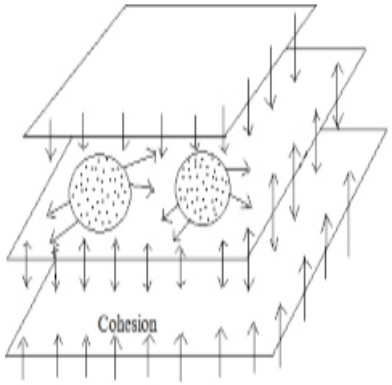

It is formed on the basis of hypothesis that translation is only made up of molecular motion. On this type, molecules are in free motion on the surface. The cohesion force is displaced. Thus, the force does not act between two molecules but somewhat between the surfaces.

Diagram of Three surface model of liquid

FOUR SURFACE MODEL OF LIQUID

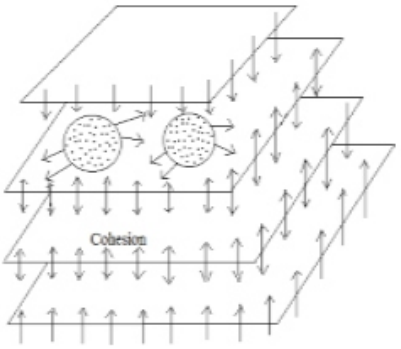

It is formed on the basis of hypothesis that translation is only made up of molecular motion. On this type, molecules are in free motion on the surface. The cohesion force is displaced. Thus, the force does not act between two molecules but somewhat between the surfaces.

Diagram of Four surface model of liquid

STRING MODEL OF LIQUID

It is formed on the basis of hypothesis rotation which is the one and only form of molecular motion which occurs in a liquid. On this type, the molecules are connected under the influence of cohesion force and subsequently gives a string structure.

String model of liquid due to cohesion force

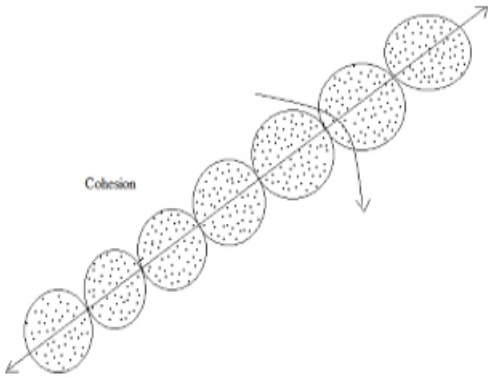

RING MODEL OF LIQUID

It is formed on the basis of hypothesis circular which is the one and only form of molecular motion which occurs in a liquid. On this type, the molecules are connected under the influence of cohesion force and subsequently gives a ring structure.

Ring structure of due to molecular motion:

There are four factors which determine the cohesional force between the molecules. They are norming, storming, performing and forming.These factors are responsible to make the molecules to attain the required shape. Even though storming makes some changes in the molecules, performing and norming binds the required factors together and help the molecules to move along a definite path.

Cohesive forces act in liquids to make them inseparable and to resist the external force. These type of forces are possible only in molecules of same substance. For example when considering rainfall, we see the rain in the form of droplets rather in the form of mist, due to the cohesion force acting in the molecules. Thus the united molecules form a large cluster which is relatively

larger in size. Thus cohesion force is considered as a intermolecular force between the molecules.

ADHESIVE FORCE AND ITS PROPERTIES

Adhesive forces are attractive forces existing between unlike molecules. These forces are mainly caused due to the mechanical forces acting between the molecules. For example in the case of glass and water, the adhesive force acting between the molecules avoids the repulsive force between the two molecules.

EFFECTS OF COHESIVE AND ADHESIVE FORCES

If we take any liquid on a smooth surface, the adhesive force acting in the molecules pulls the liquid particles down if it is stronger and the cohesive forces make the liquid molecules to maintain its original shape if it is stronger. However cohesive forces are stronger than adhesive forces in real part. The adhesive forces are stronger in water molecules, while the cohesion forces depends on the surface tension.

The shape of the liquid in any container changes when extra drops are added. The surface tension before adding the extra drops will be less and it gradually increases as the quantity of liquid increases.

CONCLUSION

Thus the various liquid molecular structures can be derived using the number of degrees of freedom. In general from the above datas we conclude that a relationship occurs between cohesion and adhesive molecules based on different factors like surface tension, area occupied by the molecules etc. This paper gives a brief study on the forces existing between the molecules in any kind of a liquid and the various diagrammatic structures like ring, string models, etc.

REFERENCES

1]. Diatomic Hypothesis and Calculation of Condensation Force by Z.Prebeg, Journal of Theoretic, Dec/Jan 2000-1 Vol.2, No. 5.

[2]. Refining the Diatomic Model for the Vaporization of liquids by G.V.Calder, Journal of Theoretics, Vol. 6-3 (2004).

[3].Theory of simple Liquids by Hansen.J.PandMcDonald.I.R, 1986- 2nd edition.

[4]. Hohenberg.P.C and Halperin.B.I, 1977 Rev. Mod. Phys.

[5]. Olsen.N.B, Christensen.T and Dyre.J.C 2001 Phys. Rev.

[6]. Hu, "Chapter 9: Friction and Adhesion," in SEDL/Manuals, Monographs and Data Series MONO7-EB / MONO10093M, ASTM Standard and Engineering Digital Library. ASTM International, West Conshohocken, Pa, USA, 2008. View at Google Scholar.

[7] G. L. Nelson, "Chapter 44: Adhesion," in MNL17-14TH-EB, ASTM International, West Conshohocken, Pa, USA, 1995.

[8] International Journal of Dentistry Volume 2012 (2012), Article ID 951324,J.Anthony Von Fraunhofer.

A Regional Geomagnetic Model Using Fourier Analysis

R. Jayapal[1], Shenu Gopal[2], C. P. Anilkumar[3] & Chandu Venugopal[2]

[1]Department of Physics,
D B College, Thalayolapparambu, Kerala - 686 605, India.
[2]School of Pure & Applied Physics,
Mahatma Gandhi University, Priyadarshini Hills, Kottayam -686560, Kerala, India.
[3]Equatorial Geophysical Research Laboratory,
Indian Institute of Geomagnetism, Krishnapuram,
Tirunelveli – 627 011, Tamil Nadu, India

ABSTRACT

We have Fourier analysed the horizontal component (H) of the Earth's magnetic field at Thiruvananthapuram (lat. 8° 29' N, long. 76° 59' E) during the years 1987 to 1998. The infinite number of terms in the Fourier expansion was truncated after the fifth term for both magnetically "quiet" and "disturbed" days.

We find that terms up to order 5 are sufficient to model the observed magnetic field at Thiruvananthapuram during both magnetically quiet and disturbed days, as there is an excellent agreement between the observed and the Fourier analysed and reconstructed fields. The seasonal and solar cycle dependence of the Fourier amplitudes have also been studied; we find the Fourier amplitudes are well correlated with the sunspot numbers.

Keywords—Geomagnetic field, Model, Fourier Analysis, Equatorial Station

INTRODUCTION

Models of the geomagnetic field use mathematical expressions to represent space and time variations of the Earth's magnetic field. Starting from the classical technique of Spherical Harmonic Analysis (SHA), first introduced by Gauss, considerable progress has been made in modelling the quiet-time, near-Earth magnetic field. For example, data from four satellites (POGO, Magsat, Orsted and Champ) were used to construct a sophisticated model that could separate out various field sources [1].

Past attempts have used Harmonic (Fourier) Analysis (HA) to model the solar quiet (Sq) variation [2, 3]. Other methods such as Rectangular Harmonic Analysis [4] , Spherical Cap Harmonic Analysis (SCHA) [5] have also been used. Spherical harmonic analyses has been further augmented by a physical method of regularization [6] and the revised Spherical Cap Harmonic Analysis (R-SCHA) [7]. Still other methods such as wavelet analysis [8] and Artificial Neural Networks (ANN) techniques [9] have

been used to model the geomagnetic daily variations.

In this paper we use the conventional HA method to model the horizontal component of the geomagnetic field observed at Thiruvananthapuram (lat 8° 29' N, long 76° 59' E) during the years 1987 – 1998. We find that the first 5 harmonics in the Fourier expansion models very well the horizontal component of the Earth's magnetic field during both geomagnetically quiet as well as disturbed days. The seasonal and solar cycle dependence of the Fourier amplitudes have also been studied.

DATAANALYSIS

As mentioned above we are interested in the HA of the horizontal component (H- component) of the Earth's magnetic field observed at Thiruvananthapuram (lat 8° 29' N, long 76° 59' E) during the period 1987 – '98. The data thus consists of 24 values of the H-component for a day.

HARMONIC ANALYSIS

A time dependent harmonic function F(t) with 24 equidistant points in the interval from t

= 0 to t = 24 (2π) can be expressed as

$$F(t_n) = \frac{A_0}{2} + \sum_{p=1}^{N/2} A_p \cos(\omega_p t) + B_p \sin(\omega_p t) \qquad (1)$$

where the time, time-step and trigonometric arguments are given by

$$t_n = n\,\Delta t \quad ; \Delta t = T/N \quad ; \omega_p t = 2\pi\, p\, n/N \qquad (2)$$

The expressions for A_0, A_p, and B_p are given by

$$A_0 = \frac{2}{N} \sum_{n=1}^{N} F(t_n)$$

$$A_p = \frac{2}{N} \sum_{n=1}^{N} F(t_n) \cos\left(\frac{2\pi p n}{N}\right) \quad ; p \neq \frac{N}{2};$$

$$A_p = \frac{1}{N}\sum_{n=1}^{N} F(t_n)\ \cos\left(\frac{2\pi n (N/2)}{N}\right)\ ;\ p = \frac{N}{2}\ ;$$

and

$$B_p = \frac{2}{N}\sum_{n=1}^{N} F(t_n)\ \sin\left(\frac{2\pi p n}{N}\right)\ ;\ p = 1, 2, \ldots \frac{N}{2} - 1 \qquad (3)$$

The amplitude C_p and phase ϕ_p of the p^{th} harmonic are then given by

$$C_p = \left[A_p^2 + B_p^2 \right]^{1/2}$$

and $$\phi_p = \tan^{-1}(B_p / A_p) \qquad (4)$$

The daily variations of the horizontal component of Earth's magnetic field can then be expressed as

$$F(t_n) = \frac{A_0}{2} + A_1\cos\left(\frac{2\pi n}{N}\right) + B_1\sin\left(\frac{2\pi n}{N}\right) + A_2\cos\left(\frac{4\pi n}{N}\right) + B_2\sin\left(\frac{4\pi n}{N}\right) + \ldots \qquad (5)$$

DATA CORRECTION

The daily variation in the H-field is not strictly periodic as required by Fourier analysis; that is, the H-value at t = 1 hour will not, in general, be the same for t = 25 hours. This difference, which is due to many factors, is corrected for in practice by applying a correction for non-cyclic behavior, the details of which are given below [10].

The base line for the H-field is defined as the average of the four values flanking local midnight (23, 24, 1 and 2 hours). The daily base line values used in this paper are:

$$H_0 = (H_{23} + H_{24} + H_1 + H_2)/4 \qquad (6)$$

where H_0 is rounded off to the nearest whole number while H_1, H_2, H_{23} and H_{24} are the hourly H-values at 1, 2, 23 and 24 hours local time respectively.

The hourly departures of the H-field from the midnight baseline value defined by (6) were obtained by subtracting (6) for a particular day from the hourly values for that particular day. Thus at "t" hours LT

$\Delta H_\tau = H_\tau - H_0$ (7) where t = 1 to 24 hours.

The hourly departure was further corrected for the noncyclic variation mentioned above. This was done by making a linear adjustment in the daily hourly values of ΔH. Thus if the hourly departures of ΔH at 01 LT, 02 LT, ……., 24 LT are denoted as V_1, V_2, ….V_{24}, thelinearly adjusted values at these hours are [10]

$$V_1 + 0\,\Delta_c,\ V_2 + 1\,\Delta_c,\ V_3 + 2\,\Delta_c,\ \ldots\ldots,\ V_{24} + 23\,\Delta_c. \qquad \text{where } \Delta_c = \frac{V_1 - V_{24}}{23}$$

Or, in other words, $\Delta H_t(V) = \Delta H_t - (t-1)\Delta_c$ (8)

Here t is the time, ranging from 01 to 24.

RESULTS

The final corrected values of the H-field, as given by (8), were Fourier analysed using (4) and reconstructed using (5), the analysis being restricted to "quiet" and "disturbed" days. The mean monthly hourly variations were arrived at by finding the mean of the hourly $\Delta H_t(V)$ values for each set of five "quiet" days of each month and similarly for the "disturbed" days.

Figure 1 is a plot of the observed data values (indicated by "continuous lines") and the Fourier analyzed and reconstructed data values (indicated by "dashed lines") versus UT for quiet days of January, 1987. The reconstructed data contains the first 5 harmonics in the Fourier seriesof (5). As can be seen from the figure, the $\Delta H_t(V)$ or H-field values increases with increasingtime, reaches a maximum between 07 - 08 UT declines sharply and reaches the baseline value by about 1500 hrs UT

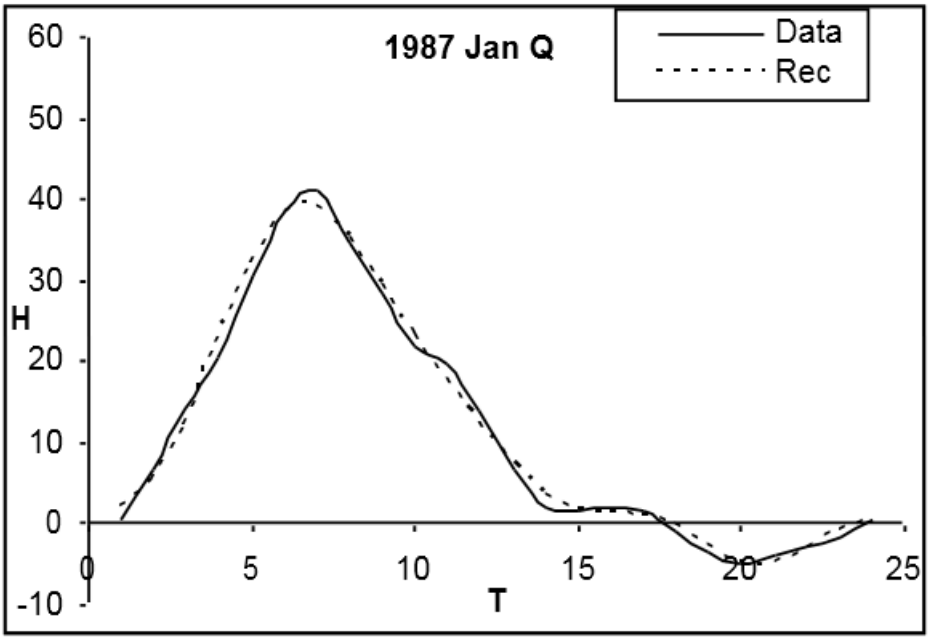

Figure 1: Plot of the measured values of the horizontal component of the earth's magnetic field (indicated by the continuous curve) and the Fourier analysed and reconstructed values (indicated by the dashed curve) for the five quiet days of January, 1987.

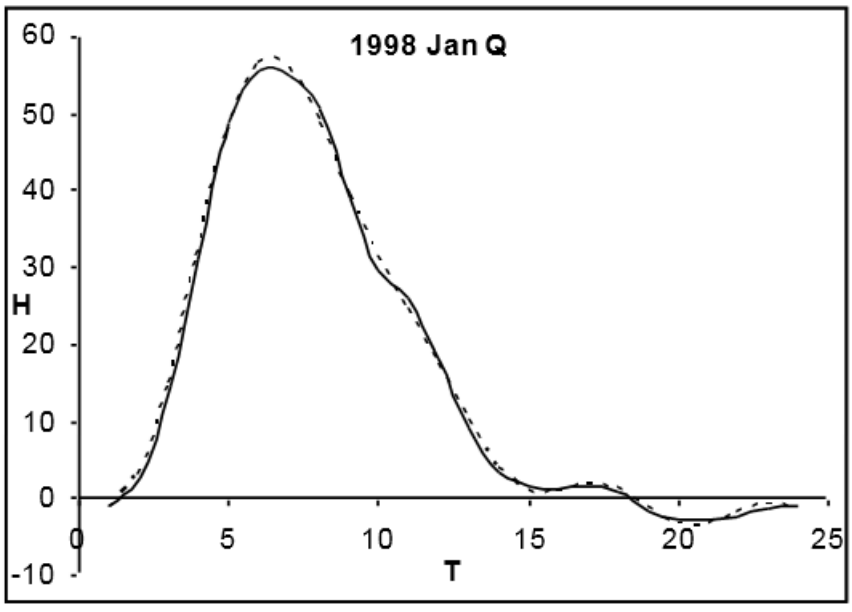

Figure 2: Plot of the measured values of the horizontal component of the earth's magnetic field (indicated by the continuous curve) and the Fourier analysed and reconstructed values (indicated by the dashed curve) for the five magnetically quiet days of January, 1998.

Figure 2, is similar to Figure 1, but for January, 1998. As is evident from the figures the agreement

the observed ΔH values and the Fourier analysed and reconstructed values are remarkably good.

The observed data values (indicated by "continuous lines") and the Fourier analysed and reconstructed data values (indicated by "dashed curves") versus UT is plotted for the month January of the magnetically "disturbed" days for the year 1987 in Figure 3, and for the year 1998 in Figure 4.

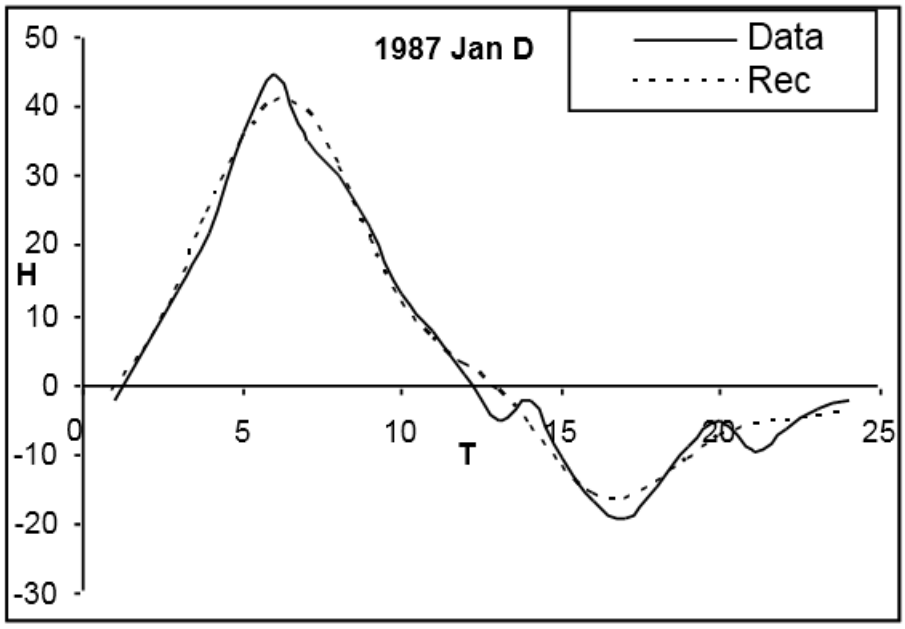

Figure 3: Plot of the measured values of the horizontal component of the earth's magnetic field (indicated by the continuous curve) and the Fourier analysed and reconstructed values (indicated by the dashed curve) for the five disturbed days of January, 1987.

Here too, the H-values reach their maximum between 07 - 08 hours UT as in the case of quiet days. However, in contrast to quiet days, the horizontal component exhibits large excursions on the negative side around local noon before returning to the baseline values. Similar curves were drawn for all the twelve months for the rest of the years.

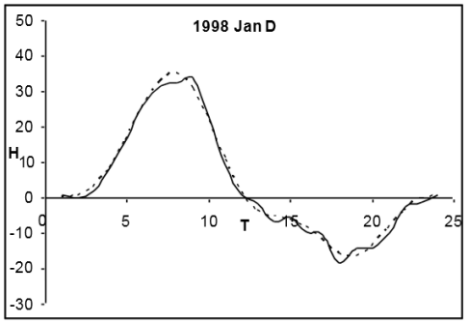

Figure 4: Plot of the observed values of the horizontal component of the earth's magnetic field (indicated by the continuous curve) and the Fourier analysed and reconstructed values (indicated by the dashed curve) for five disturbed days of January, 1998.

SEASONAL VARIATIONS OF THE COEFFICIENTS

In this section we study the seasonal variations of the coefficients of the Fourier series (3). We follow the Lloyd's seasons [11] and divide the months of the year into three seasons: December or D-season (January, February, November and December), Equinox or E-season (March, April, September and October) and the June solstice or J-season (May, June, July and August).

Thus Figures 5 and 6 are plots of the leading coefficients in the series (5) versus the years studied, with A_0, A_1 and A_2 being given in figure 5 and B_0, B_1 and B_2 in figure 6. As can be seen from figure 5, the coefficient A_0 which is representative of the background magnetic field is highest during the E- months. The same is true for the second order coefficient A_2, while the first order coefficient A_1 shows a mixed behavior. On the other hand, A_0 during the D and J months does not show any consistent behavior, with A_0 for the D-months being less than equal to or greater than the A_0 values for the J-months. The same is also true for the coefficients A_1 and A_2 for the D and J-months.

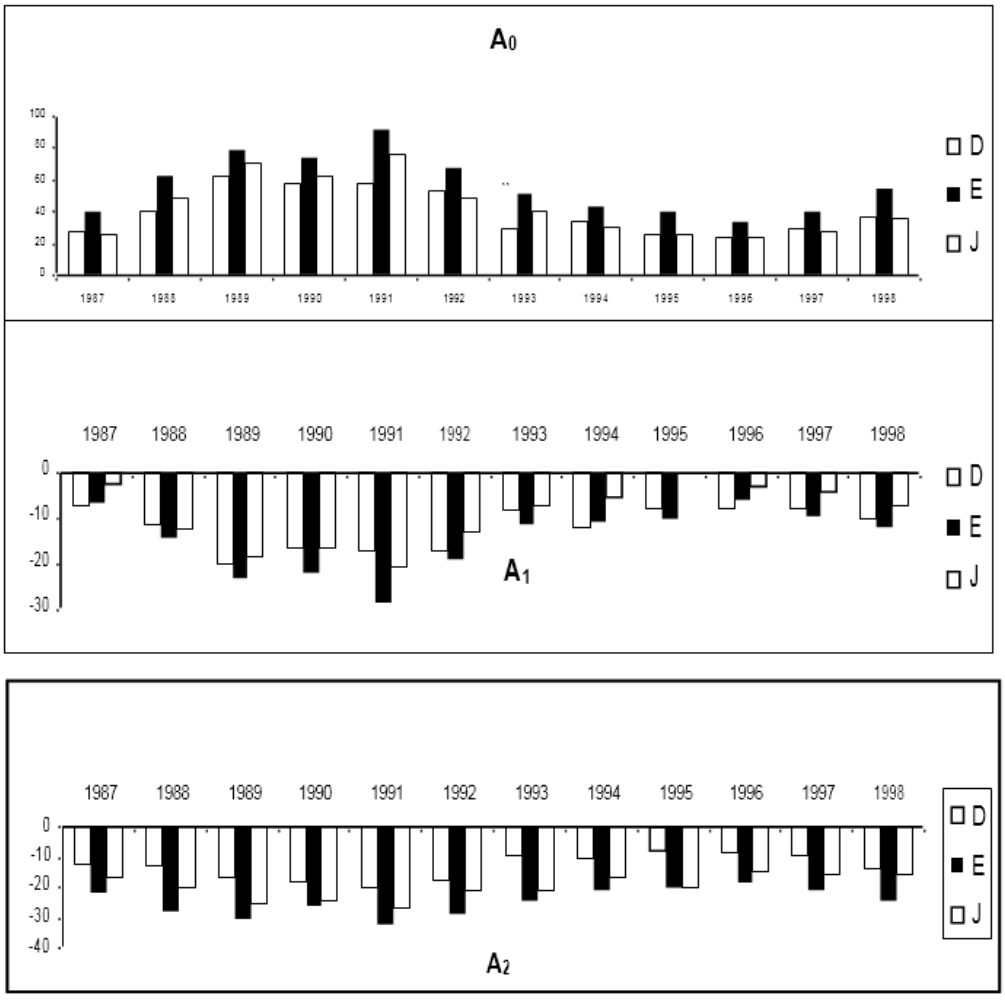

Figure 5: Plot of the variation of the zero (A_0), first (A_1) and second (A_2) order Fourier coefficients of (5) versus time (in years) as a function of the seasons.

Similar to A_0 in figure 5, the coefficient B_1 (figure 6) dominates during the E-months. The same is also true for the third order coefficient B_3; while the first order coefficient shows a mixed behavior, B_1 for the J-months is generally greater than B_1 for the D-months (except for 1998 when it is slightly lower). Similarly the coefficients B_3 is generally dominant for the E- months (except for 1995). Also B_3 for the D-months is the least, except for 1992 when it is slightly greater than B_3 for.

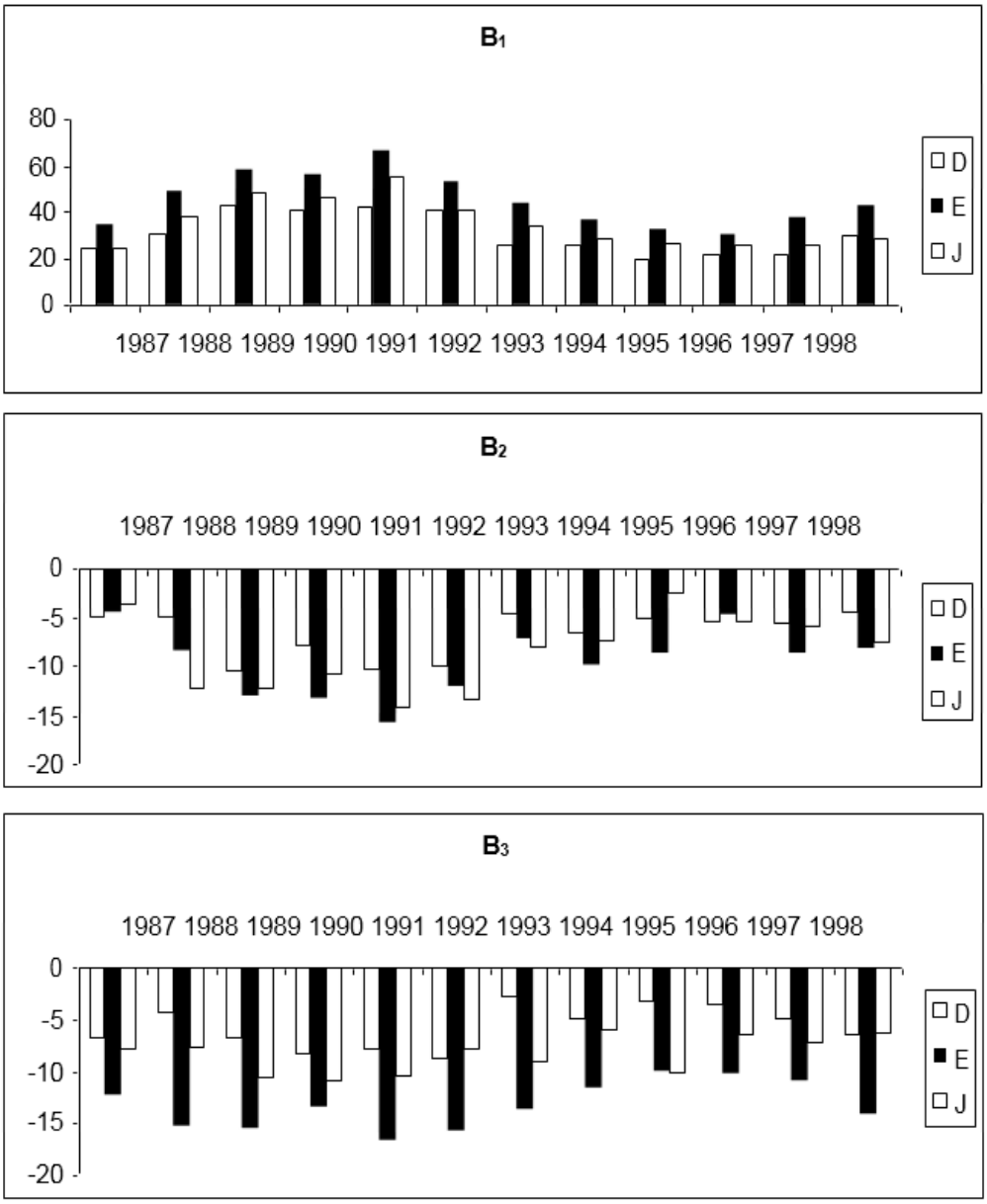

Figure 6: Plot of the variation of the first (B_1), second (B_2) and third (B_3) order Fourier coefficients of (5) versus time (in years) as a function of the seasons.

D-months. Finally, figure 7 depicts the plot of the coefficients A_0 and B_1 with sunspot number for the years 1987-'98. As can be seen from the figure both the coefficients A_0 and B_1 correlate positively with the sunspot number.

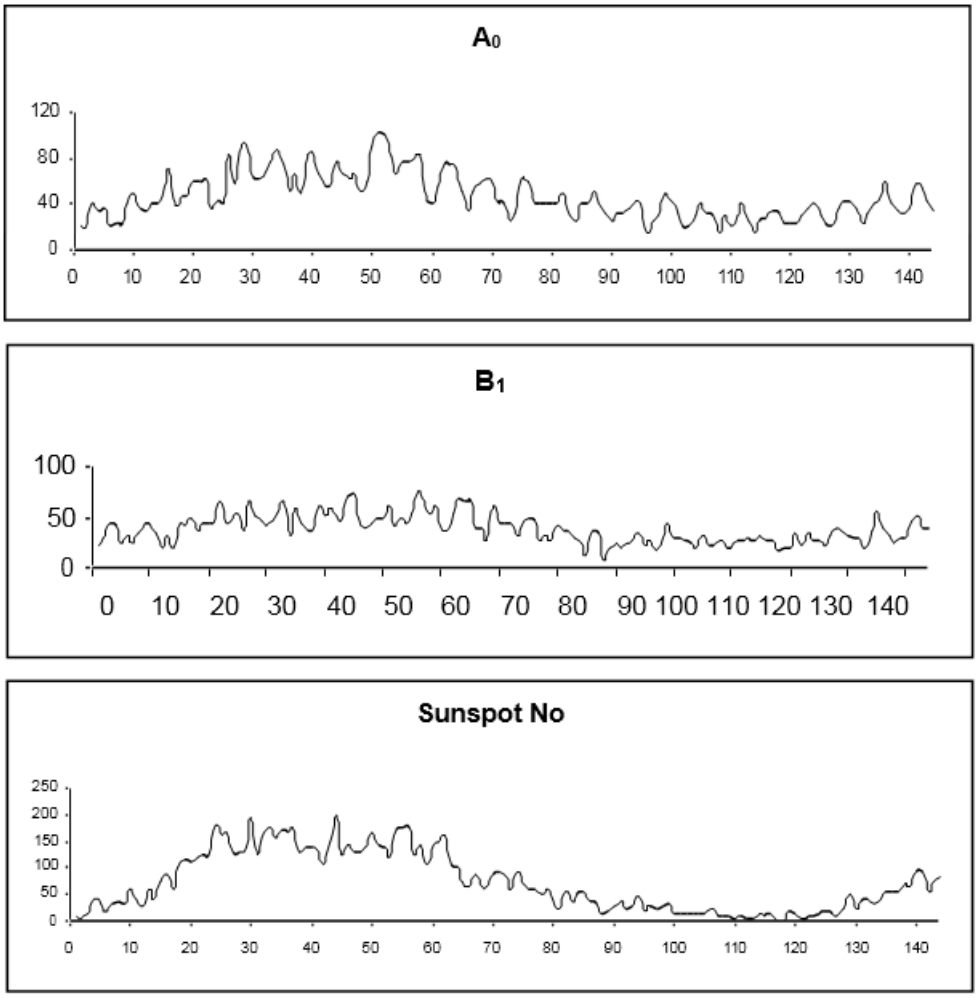

Figure 7: Plot of the Fourier coefficients A_0 and B_1 of (5) and the sun-spot number versus time from 1987 to 1998 (depicted as cumulative months from 0 to 144).

DISCUSSION

The daily variation of the Earth's magnetic field is known to be generated by solar heating in the upper regions of the atmosphere; this is due to the movement of conductive air across the lines of the magnetic field. However, Schruster [12] and Chapman [13] suggested lunar and solar tides as the cause of air movement in the upper atmosphere, which is associated with the dynamo current and driven by wind and thermal tidal motions in the E-region of the ionosphere. Due to the presence of a non-conducting boundary, a strong vertical polarisation field opposes the downward flow of electric current. This field, in turn, gives rise to an

intense Hall current which has been named as the equatorial electrojet (EEJ) [14]. This EEJ flows along the dip equator in the ionospheric E-region on the dayside within a latitudinal belt of ± 3° and is responsible for the variations observed in the Earth's magnetic field.

On disturbed days, however, it has been suggested that the enhancement of the field over the magnetic equator during storm sudden commencement is due to the imposition of an additional electric field over the equatorial region, causing additional electrojet currents [15].

An additional mechanism is the thermospheric winds produced by auroral heating during magnetic storms. These westward winds drive an equatorward Pedersen current which ultimately results in the generation of a poleward electric field, a westward drift and an eastward current. This total pattern of disturbance winds, electric fields and currer $\bar{E} \times \bar{B}$ superimposed upon the background quiet day pattern [16]. These neutral winds can also spread their influences to lower latitudes even in the absence of electric fields through Joule heating coupled to convective ion drag and Corioli's force [17, 18] . And anomalously high wind speeds have been observed on numerous occasions at mid-latitudes during disturbed conditions.

The zero order coefficients in the Fourier series expansion of the geomagnetic field is a measure of the stationary component present at all times. The plasma densities in the ionosphere vary greatly between day and night as well as with season, solar activity and solar cycle. The daily variation of the electron densities aids the development of ionospheric currents which contribute to the diurnal magnetic field variations observed at the surface; the first order coefficients are thus a measure of this diurnal variation. While it is tempting to interpret the higher periods as artefacts of the Fourier series expansion, it may be noted that thermospheric winds have been observed with periods of 45 and 58 hours; one of the stations' data that contributed to this study was that of Alibag. These thermospheric winds can move ionospheric plasma across geomagnetic field lines creating a dynamo that can set up currents which can modulate the field at these higher periods [19]. As regards variation with season it may be noted that Rastogi and Iyer [20] , in a study of the quiet day variations of the geomagnetic field at low latitudes, found the variations in amplitude to be a maximum during the equinoctial months. We also find the Fourier coefficients to be generally larger during the E-months. Finally, in a study of the quiet day geomagnetic field at 21 stations, Yamazaki et. al. [21] have shown that the quiet day variations very emphatically depend on solar activity. While the F10.7 radiation was their proxy for solar activity, we find that the Fourier coefficients (and hence the field deviations) correlate positively with Sun spot number.

CONCLUSION

We have, in this paper, modelled the horizontal component of the Earth's magnetic field observed at Thiruvananthapuram by Fourier analysis, retaining the first five harmonics in the Fourier expansion.

We find that the first five harmonics are sufficient to model the horizontal component of the Earth's magnetic field observed at Thiruvananthapuram, as there is excellent agreement between the observed and the Fourier analysed and reconstructed values on “quiet days”; minor deviations occur on “disturbed days” due to the rapid fluctuations in the H-field on such days.

ACKNOWLEDGEMENTS

RJ and CVG thank the UGC, New Delhi for a Teacher and Emeritus Fellowship respectively.

REFERENCES

1. *T J Sabaka, N Olsen, and M E Puruckel, 2004 Extending comprehensive models of the Earth's magnetic field with Orsted and CHAMP data . Geophys. J. Int. doi 1111/j 1365- 266X.2004.02421.x*
2. *W H Campbell and E R Schiffmacher 1985. Quiet ionospheric currents of the northern hemisphere derived from geomagnetic field records. J. Geophys Res., 90, 6745 - 6486.*
3. *W H Campbell and E R Schiffmacher 1988 Quiet ionospheric currents of the southern hemisphere derived from geomagnetic field records. J. Geophys Res., 93, 933 - 944.*
4. *L Alldredge 1981. Rectangular harmonic analysis applied to the geomagnetic field. J. Geophys. Res., 86, 3021 - 3026.*
5. *G V Haines 1985. Spherical cap harmonic analysis. J. Geophys. Res., 90, 2583 – 2591*
6. *M Korte and R Holme 2003 Regularization of spherical cap harmonics. Geophys. R. Int. 153, 253 – 262.*
7. *E Thebault, J Schott. M Mandea and J Hoffbeck 2005. A new proposal for spherical cap harmonic modeling. Geophys. J. Int. 159 83 – 103.*
8. *M Holschneidner, A Chambodut and M Mandea 2003. From global to regional analysis of the magnetic field on the sphere using wavelet frames. Phys. Earth Planets In. 135 107 – 124.*
9. *P R Sutcliff 1999 The development of a regional geomagnetic daily variation model using neural networks. Ann. Geophysicae, 18, 120 - 128.*
10. *A B Rabiu, A I Mamukuyomi and E O Joshua, 2007. Variability of equatorial ionosphere inferred from geomagnetic field measurements. Bull. Astr. Soc. India, 35, 607- 618.*
11. *F Eleman, 1973. Cosmical Geophysics, ed. Egeland A et al, Scandinavian University Books, Oslo, Chapter 3, 45.*
12. *A Schruster, 1908 The diurnal variation of terrestrial magnetism. Philos. Trans. Roy. Soc. London A. 208 163 – 204.*
13. *S Chapman, 1919 The solar and lunar diurnal variations of terrestrial magnetism. Philos. Trans. Roy. Soc. London A. 218, 1 – 118.*
14. *S Chapman, 1951 The equatorial electrojet as detected from the abnormal electric current distribution above Huancayo and elsewhere. Arch. Meteorl. Geophys. Bioclimatol. A 4, 368 – 392.*
15. *S Rastogi, 1976. Equatorial E-region electric field changes associated with a geomagnetic storm sudden commencement. J. Geophys. Res. 81 687 – 689*
16. *M Blanc, and A D Richmond, 1980. The ionospheric disturbance dynamo. J. Geophys. Res. 85, 1669 – 1686.*
17. *P W Roper, and A J Baxter, 1978 The effect of auroral energy input and ion drifts in the thermosphere. J. Atmos. Terr. Phys. 40 585 - 599*
18. *M Strauss, 1978 Dynamics of the thermosphere at high latitudes. Rev. of Geophys. 16 183 – 194.*
19. *M Takeda and Y Yamada, 1989 Quasi Two-Day Period Variation of the Geomagnetic Field. J Geomag. Geoelectr. 41 469 – 478*
20. *R G Rastogi and K N Iyer, 1976 Quiet day variation of the geomagnetic H-field at low latitudes. J. Geomagnetn. Geoelectr. 28, 461 - 479.*
21. *Y Yamazaki, et. al., 2011. An empirical model of the quiet daily geomagnetic field variation. J. Geophys. Res. v. 116 doi: 10.1029 / 2011 JA 016487*

Thickness Dependent Coercive Field And Magnetic Anisotropy In Cofeb Thin Films

Kailash Chandra[1,] Dr. Hemant Kumar[2], Sachin Kumar[3]
[1,2,3]Department of Physics, Motilal Nehru College (University of Delhi) Benito Juarez Marg New Delhi – 110021, India

A B S T R A C T

Transition metal–metalloid (TM–M) alloy CoFeB is an amorphous soft ferromagnetic material. The structural and magnetic properties of as-grown 6–24 nm thin magnetron sputtering deposited $Co_{20}Fe_{60}B_{20}$ films are reported in this communication. We report the magnetization behavior of the as-deposited sputtered CoFeB films synthesized at 300 K. The longitudinal Magneto-Optic Kerr Effect measurements achieved at 300 K in these as-grown films clearly established increase in the coercivity with the increase of the film thickness. The coercivity is increasing due to the annealing of thin films at 300° C. The X-ray measurement of as-deposited Si/CoFeB thin films indications that the as-deposited film is amorphous whereas after 300° anneal it become crystalline bcc CoFeB as it obvious from the clear presence of the diffraction peak at 2θ ~ 44.8° attribute to (110) plane.Study of their magnetization behaviour by MOKE measurement for examinations of anisotropy measured at different angles between the applied field H and the uniaxial anisotropy axis (0°) of the film and find easy axis (0°) & hard axis (90°). We have estimated the magnetic anisotropy by evaluating the anisotropy field H_k (θ) is found to increase from θ = 0° to 90° thus magnetization behavior in this film is telling of certain existence of in plane uniaxial anisotropy (K_u).

Keywords—Magnetization, MOKE, CoFeB thin film, uniaxial anisotropy and As-deposited.

1.0 INTRODUCTION

Ultrathin ferromagnetic (FM) thin films are the basic key of the Spintronic devices due to the fact that the direction of magnetic easy-axis and strength of magnetic anisotropy in these films can be manipulated by underlying buffer layer, external magnetic field for the period of growth, deposition and magnetic annealing[1–3]. The magnetic properties of these materials are the result of the competition between the ferromagnetic exchange interaction and the magnetocrystalline anisotropy of each site. The magneto-crystalline anisotropy will try to rotate the spin moment to the direction of anisotropy of each particular site whereas the exchange coupling will try to align the spins from site to site. As aoutcome, the spins will be spatially interconnected (aligned) over a characteristic length that will be longer the stronger is the exchange interaction compared to the magneto-crystalline anisotropy. The magnetization behavior of such films is likely to add to the appreciative of the complex participation of domains in the

magnetization procedure.[4]

The ferromagnetic CoFeB alloy is an amorphous soft material. It steadily recrystalline at annealing above a temperature which depends on its composition.The CoFeB is a strongly utilizable material in spintronics devices such as in magnetic tunnel junctions (MTJs), sensor applications, magnetic random access memories (MRAMs) and other novel devices [5-6].CoFeB in concurrence with AlO[7-8] and recently with MgOhas been shown to reveal a record high tunnel magneto resistance (TMR) values at room temperature. In such devices, the in-plane magnetic anisotropy of the CoFeB films is a required property for their process. Long-range nature is not necessary for a material to demonstrate ferromagnetic properties because of the nature of the exchange interaction, short-range nature is far more momentous. The structural and magnetic properties of as-grown 6–24 nm thin magnetron sputtering deposited transition metal– metalloid $Co_{20}Fe_{60}B_{20}$ (CFB) films are reported in this paper. CoFeB films can be either amorphous or crystalline, depending on the boron content, seed layers, film thicknesses and magnetic thermal treatment. This was investigated by Cardoso *et.al* [9].In the current report, the structural and magnetic properties of the as deposited single layer soft ferromagnet *CoFeB* of different thicknesses is investigated by using MOKE SET UP (to investigate magnetic properties) and GAXRD (to investigate the structural properties).

2. EXPERIMENTAL DETAILS

Single layer $Co_{20}Fe_{60}B_{20}$(x) films (where x = 6nm, 14nm, 20nm and 24 nm) are deposited bydc-magnetron sputtering system on Si (100) substrate. Before the deposition, substrates were cleaned first with acetone and then propane in ultrasonic bath. Deposition was carried out at 1×10^{-3}torr pressure and 50 watts DC power in argon gas environment (30 sccm) at room temperature. The deposition rate is estimated (~ 0.034 nm / sec) by knowledge of film thickness and depositiontime. The grown films were further annealed at 300 °C for 60 min in 4×10^{-6}torr vacuum.As-deposited and annealed samples were characterized for structural and magnetic properties using versatile techniques. Structural characterization is carried out with glancing angle X-ray diffraction (GAXRD). Hysteresis loop and hence magnetic properties of as- deposited and annealed samples were characterized at room temperature using magneto optical Kerr effect (MOKE). MOKE measurement was recorded in longitudinal geometry where direction of magnetic field is both in plane and perpendicular to laser incident beam (where laser beam is in s-polarized state).

3. RESULT AND DISCUSSION

X-Ray Diffraction Analysis

Fig.1 (a & b) shows GAXRD measurement of as-deposited and 300 °C annealed CoFeB thin film (24nm). The featureless XRD pattern observed for *as-deposited* thin film shows amorphous nature of the film[10-11]. The presence of diffraction peak at 44.7°for the films annealed at 300 °C is attributed to (110) plane with bcc structure[12-13]. This is clear evidence of the fact that annealing leads to conversion in amorphous to crystalline nature. Furthermore, increase in films thickness results in the enhancement in crystalline nature due to increase in peak intensity (or reduction in FWHM). The reduction in FWHM indicates an increase in grain size which is estimated using Scherer's formula

$$D = \frac{0.89\,\lambda}{\beta cos\theta}$$

Where D is crystallite size,l wavelength of X-ray used (1.54 Å) and b is FWHM and q is Bragg's angle.

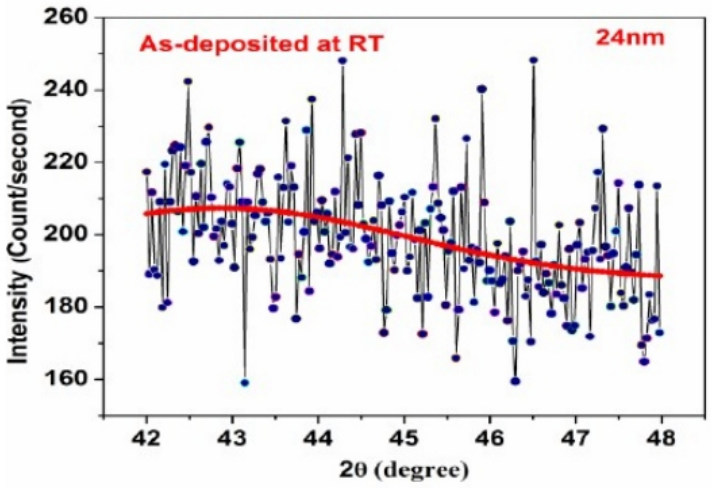

Fig. 1 (a) XRD scan of *as-deposited* CoFeB thin film (24 nm) exhibiting amorphous nature

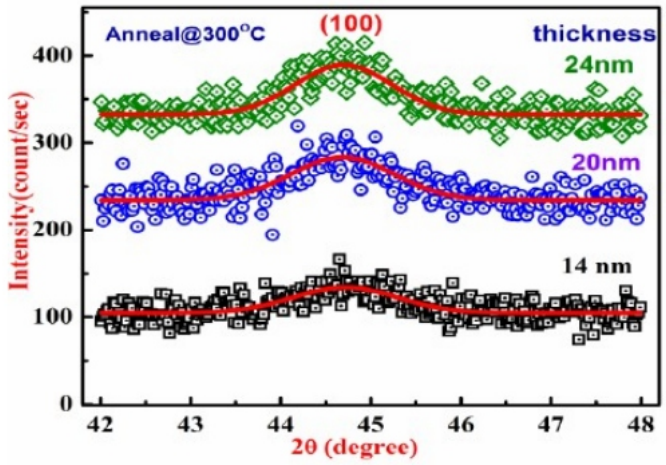

Fig.1 (b) XRD pattern of CoFeB thin films (14 nm, 20 nm and 24 nm) annealed at 300°C.

MAGNETO-OPTIC KERR EFFECT

Magnetic characterization (M–H loop) was carried out at room temperature using longitudinal magneto-optic Kerr effect (L-MOKE) magnetometer (Fig. 2). MOKE works on the principle that the interaction of polarized light with a magnetic sample governs the change in polarization of light. In L-MOKE system, magnetic field orientation is perpendicular to the plane of incidence and parallel to the surface of sample.

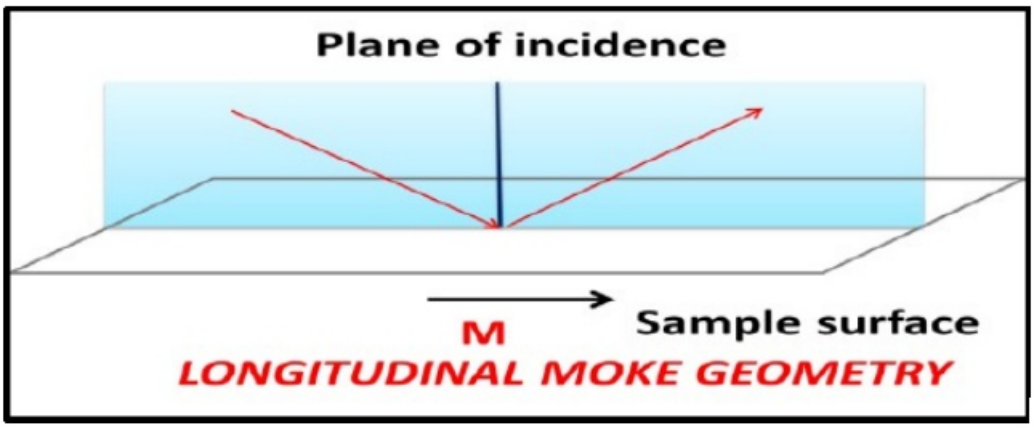

Fig.2 Schematic representation of Longitudinal MOKE (L-MOKE) Geometry

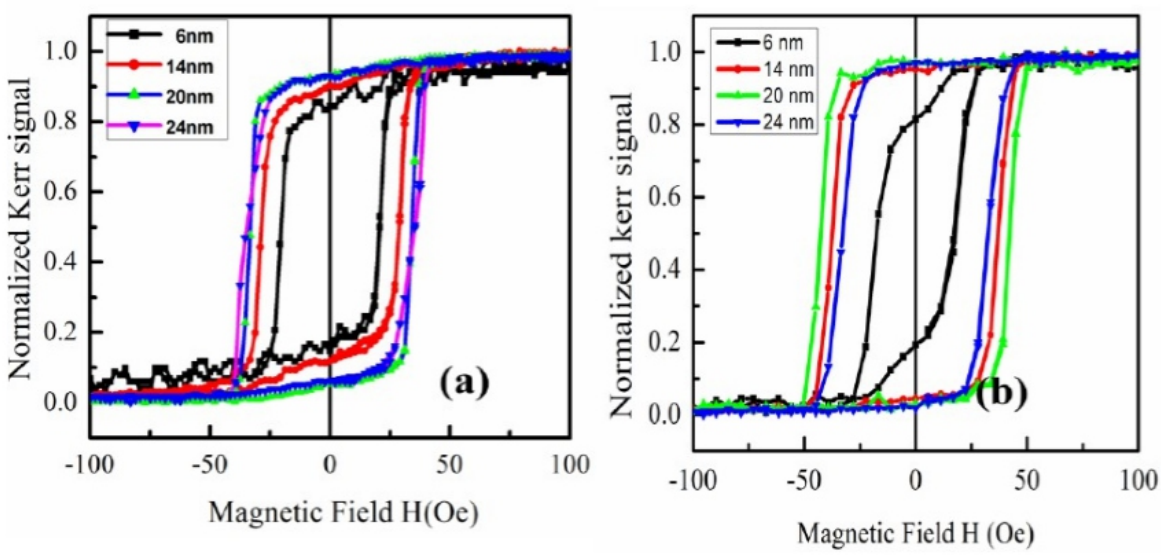

Fig. 3 MOKE M-H loops of CoFeB thin films having thickness 6 nm, 14 nm, 20 nm& 24 nm(a)*as-deposited*& (b) annealed at 300 °C.

THICKNESS DEPENDENCE MAGNETIZATION STUDY

The magnetic loops for Co20Fe60B20 thin films (*as-deposited* and annealed) obtained using L-MOKE technique are presented in Fig. 3**.** Well-defined coercive (Hc) behaviour in magnetization loop shows transition from one saturated magnetic state to oppositely saturated magnetized state. The coercivity(Hc) values for *as-deposited* films having thickness 6 nm, 14 nm, 20 nm and 24 nm are found to be ~ 20 Oe, ~ 28 Oe, ~33 Oe and ~34 Oe respectively.

Magnetic measurements were again carried out on these samples after vacuum annealing at 300 C. In this case, coercivity(Hc)value for 6 nm film annealed at 300 °C is ~17 Oe. The increase in thickness i.e. for 14 nm & 20 nm leads to boost in coercive values (~ 37 Oe and ~ 42 Oe) respectively. Further, increase in film thickness is expected to cause increase in grain size and hence reduction of grain boundaries. Generally in thin films, grain size is proportional to film thickness.The observed XRD patterns, as discussed earlier (Fig. 1) indicate that *as-deposited* CoFeB film is amorphous, whereas annealed CoFeB films are crystalline in nature. It can be concluded there is an enhancement in film-crystallinity and coercivitydue to annealing in comparison to as-deposited CoFeB thin films. However for 24 nm thick film annealed at 300 °C shows reduction in Hc value (~32 Oe) as can be seen from (Fig. 4). This may be attributed to multi-domain behavior of thin films at higher thicknesses.

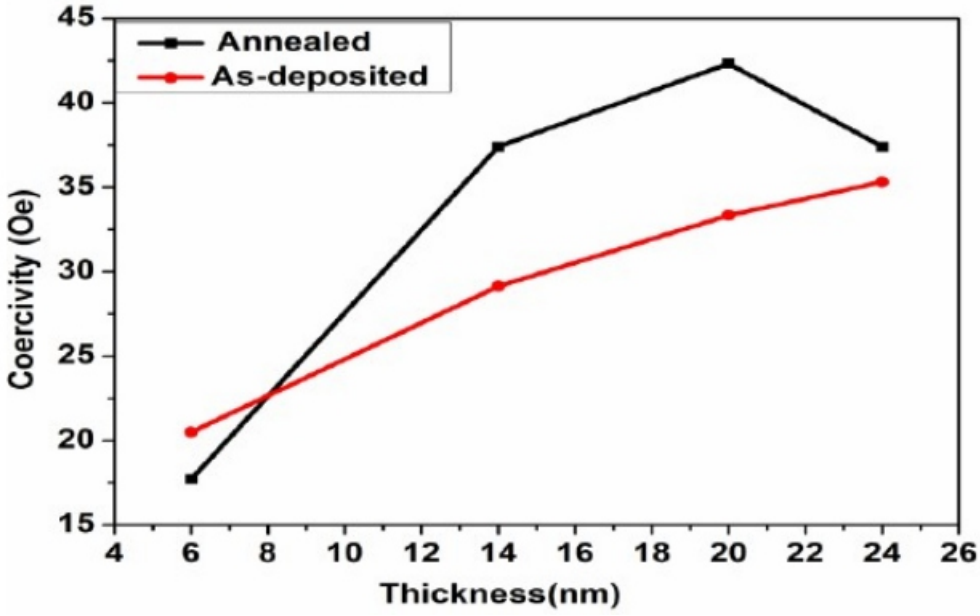

Fig. 4 Variation of coercivity (H_c) with film thicknesses (t) for *as-deposited* and 300°C annealed CoFeB thin films.

ANGULAR DEPENDENCE OF MAGNETIZATION REVERSAL MECHANISM

To further study the nature of magnetic anisotropy, MOKE measurements were carried out at different angles lying between q=0° to90°[14]. Fig. 5(a) shows such a data for 24nm CoFeB thin film. The growth of magnetization in hysteresis loop is attributed to systematical change from the sharp reversal. The gradual change in saturation with increasing angle from q=0° to q=90°essentially involves the rotation of domain walls.

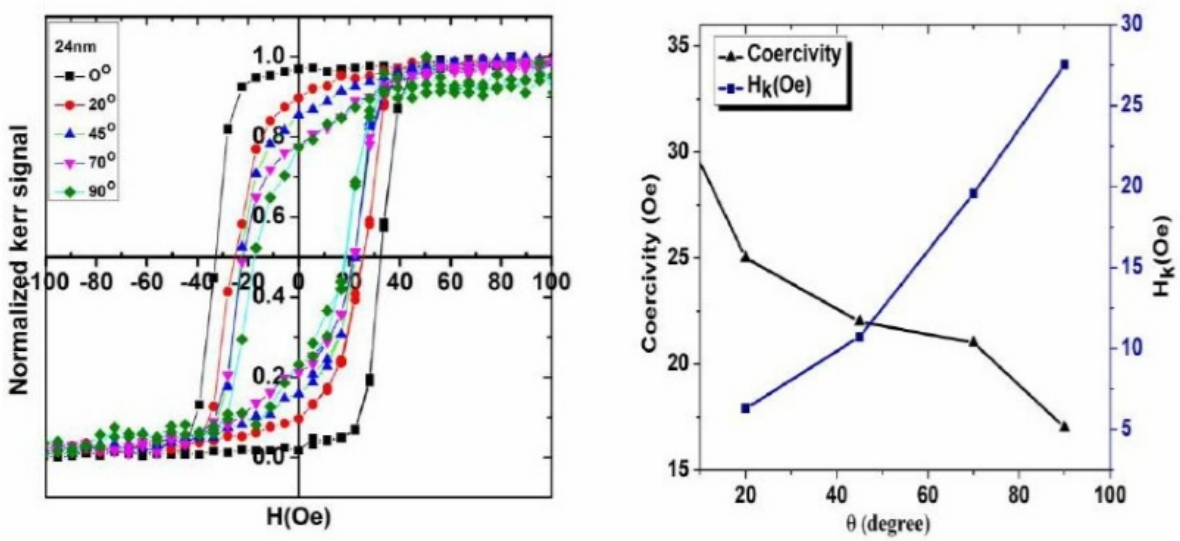

Fig. 5(a) MOKE M-H loops of Si/CoFeB (24nm) film, measured at different angles between applied magnetic field direction and the easy axis.(b) Variation of anisotropy field H_k(q) and coercivity with angle (q) between easy and hard axis for 300°C annealed CoFeB film (24 nm).

Reports have shown thatmagnetic anisotropy is calculated by knowing the anisotropy field (H_k) which is given by difference between saturation field at angle θand easy axis θ=0°[15-17].

$$H_k(\theta) = H_{sat}(0^0) - H_{sat}(\theta) \qquad (1)$$

Fig. 5(b) shows the variation in anisotropy field H_k (q)for 300°C annealed CoFeB film (24 nm). (q) is found to increase with the increase in angle from q=0° to 90°. The existence of magnetic behaviour in 300°C annealed CoFeB film reveals the presence of in-plane uniaxial magnetic anisotropy (K_u) estimated using following equation

$K_u = H_k M_s/2$ (2)

Here, $H_k$and M_s are the anisotropy field and saturation magnetization respectively. The magnetization curve follows Stoner-Wolfarthsingle domain magnetization reversal mechanism. It shows a complete or near complete alignment of ferromagnetic spins along the direction of applied field. Further, the coercivity of 300°C

annealed CoFeB film (24 nm) is found to be maximum when the applied field is aligned parallel to the direction of easy axis (θ=0°) and reduces along the hard axis (θ=90°). The magnetization reversal starts as early as the angle between easy axis and field is gradually increasedresulting in reduced coercivity with increasing angle (see Fig.5b). This indicates that forθ = 90°,low field are required to reduce the net magnetization of film to zero. Thus, the coercivity essentially measures the resistance by theferromagnetic film from becoming demagnetized.

4. CONCLUSION:-

Structural and magnetic properties of *as-deposited* and annealed CoFeB films of four different thicknesses (6nm, 14nm, 20nm and 24nm) were studied by GAXRD and MOKE respectively. After vacuum annealing at 300°C, the films exhibited poly-crystalline nature with bcc structure of CoFeB, as was evident from the clear presence of the diffraction peak at 2q~44.7° The grain size was found to increases with the increase in film thickness.It was observed that the coercivity increases with the increase in thicknesses of the as-deposited films. The coercivity exhibited noticeable decrease on annealing for film thickness greater than 20nm. This was attributed to multi-domain behavior of thin films at higher thicknesses.The MOKE M- H measurements showed the presence of magnetic anisotropy in the measured sample. The anisotropic field H_k (θ) is found to increase as the field was oriented away from the easy direction, i.e., from q=0° to 90°. This behavior of the magnetization in the annealed film is reveal of the existence of in plane uniaxial anisotropy (UMA).

5. REFERENCES:-

1. *N. Martin, J. McCord, A. Gerber, T. Strache, T. Gemming, I. Monch, N. Farag, R. Schafer, J. Fassbender, E. Quandt, and L. Schultz, Appl. Phys. Lett.* ***94****, 062506 (2009).*
2. *J. Fassbender and J. McCord, J. Magn. Magn. Mater.* ***320****, 579 (2008).*
3. *B. Cui, C. Song, Y. Y. Wang, W. S. Ya, F. Zeng, and F. Pan, J. Phys. Condens. Matter.* ***25****, 106003 (2013).*
4. *Z.-H. Wang, G. Cristiani, H.-U. Habermeier, and J. A. C. Bland, Phys. Rev. B* ***72****, 054407 (2005).*
5. *D. D. Djayaprawira, K. Tsunekawa, M. Nagai, H. Maehara, S. Yamagata, N. Watanabe, S. Yuasa, Y. Suzuki, and K. Ando, Appl. Phys. Lett.* ***86****, 092502 (2005).*
6. *T. Uhrmann, T. Dimopoulos, H. Brückl, V. K. Lazarov, A. Kohn, U. Paschen, S. Weyers, L. Bär, and M. Rührig, J. Appl. Phys.* ***103****, 063709 (2008).*
7. *D.W. Nordman, C. Daughton, J.M. Zhenghong, Q. Fink, IEEE Trans.Magn.****40*** *2269(2004).*
8. *I.Gubanov, Sov. Phys. Solid State* ***2****, 468 (1960).*
9. *S. Cardoso, C. Cavaco, R. Ferreira, L. Pereira, M. Rickart, P. P. Freitas, N. Franco and N. P. Barrada, J. Appl. Phys.* ***97****, 10C916 (2005).*

10. *C. Park, Y.-H. Wang, D. E. Laughlin and J.-G. Zhu, IEEE Trans. Magn.* ***42****, 2639 (2006).*

11. *Y. Zhang, X. Fan, W. Wang, X. Kou, R. Cao, X. Chen, C. Ni, L. Pan, and J. Q. Xiao, Appl. Phys. Lett.* ***98,*** *042506 (2011).*

12. *S. Cardoso, C. Cavaco, R. Ferreira, L. Pereira, M. Rickart, P. P. Freitas, N. Franco and N. P. Barrada, J. Appl. Phys.* ***97****, 10C916 (2005).*

13. *R. Lavrijsen, P.V. Paluskar, C.T.J. Loermans, P.A. van Kruisbergen, J.T. Kohlhepp, H.J.M. Swagten, B. Koopmans, E. Snoeck, J. Appl. Phys.* ***109****093905 (2011).*

14. *Z. L. Han, J. H. Ai, P. Zhan, J. Du, H. F. Ding, and Z. L. Wanga, Appl. Phys. Lett.* ***98****, 031903 (2011).*

15. *M. Raju, S. Chaudhary and D.K. Pandya, J. Appl. Phys.* ***114****, 053911 (2013).*

16. *L. Kipgen, H. Fulara, M. Raju and S. Chaudhary, J. Magn. Mag. Mater.* ***324****, 3118(2012).*

17. *J. Diaz, N.M. Hamdan, P. Jalil, Z. Hussain, S.M. Valvidares, J.M. Alameda, IEEE transactions on Magnetics* ***38****, 2811 (2002).*

Synthesis And Characterization Of Lead Ii Iodide Nanoparticles

R. Hepzi Pramila Devamani[1] , A. Akila[2] & M.Indhumathi[2]

[1.] Assistant Professor, Department of Physics, V.V.Vanniaperumal College for Women

[2.] M.Sc Students, Department of Physics, V.V.Vanniaperumal College for Women, Virudhunagar.

A B S T R A C T

Lead II Iodide nanoparticles were synthesized via chemical co-precipitation method from lead (II) nitrate and sodium iodide. The formed nanoparticle is characterized by powder x-ray diffraction, scanning electron microscopy, ultra-violet spectroscopy and fourier transform infrared spectroscopy, confirmed the preferential growth of lead II iodide nanoparticles that width is 30.8 nm. The SEM image shows the synthesized lead II iodide show well crystallized particles with spherical morphology. The FTIR spectrum is used to study the stretching and bending frequencies of molecular functional groups in the sample. From UV spectrum, the band gap of lead II iodide nanoparticles is found to be 3.5eV.

Keywords—XRD, SEM, FTIR, UV.

INTRODUCTION

Nanotechnology is concerned with synthesis of nanoparticles of various size, shape and chemical composition and their potential use. Nanomaterials have created high interest in recent years by virtue of their unusual mechanical, electrical, optical and magnetic properties. Lead nanostructures are attractive materials for its applications such as lead batteries and catalysis. Lead II iodide is used for recording optical images; for making gold spangles and mosaic gold for decorative purposes; in photographic emulsions; in mercury-vapor lamps; in asbestos brake linings; in far-infrared filters; in thermal batteries; in printing and recording papers; and in aerosols for cloud seeding. This paper deals with easy, simple, fast and low cost synthesis of lead II iodide nanoparticles by chemical co-precipitation method and its characterizations.

MATERIALS AND METHODS

Nanoparticles of lead II iodide were prepared by chemical co precipitation method by adding lead (II) nitrate and sodium iodide. Precise amounts of reagents taking into account their purity were weighed and dissolved separately in distilled water into 0.1M concentration. After obtaining a homogeneous solution, the reagents were mixed using magnetic stirring. The precipitate was separated from the

reaction mixture and washed several times with distilled water and ethanol. The wet precipitate was dried and thoroughly ground using agate mortar to obtain the samples in the form of fine powder [1].

TESTS CONDUCTED

X-ray diffraction is an ideal technique for the determination of crystallite size of the powder samples. The basic principle for such a determination involves precise quantification of the broadening of the peaks. XRD line broadening method of particle size estimation was chosen in this investigation for determining the crystallite size of the powder sample. The morphology of the powder samples was studied by the scanning electron microscope (SEM) analysis. The infra red spectroscopic (IR) studies of lead II iodide nanoparticles were made by using 'SHIMADZU' FTIR 8400S model spectrometer through KBr method. The UV spectrum was taken in the absorbance mode in the wavelength range from 200 to 800 nm.

RESULTS AND DISCUSSION

XRD STUDIES

XRD – PARTICLE SIZE CALCULATION

The XRD patterns of the prepared samples of lead II iodide nanoparticles are shown in figure.1. XRD studies reveal that the samples are nano sized and crystalline. The fine particle nature of the samples is reflected in the X-ray line broadening. The size of the synthesized lead II iodide nanoparticles are calculated using Scherrer equation

$$D = 0.9\lambda / \beta \cos\theta \qquad (1)$$

where λ represents wavelength of X rays, β represents half width at full maximum and θ is the diffraction angle[2]. The average grain size of the particles is found to be 30.8 nm. The XRD pattern of lead II iodide nanoparticles is shown in figure 1.

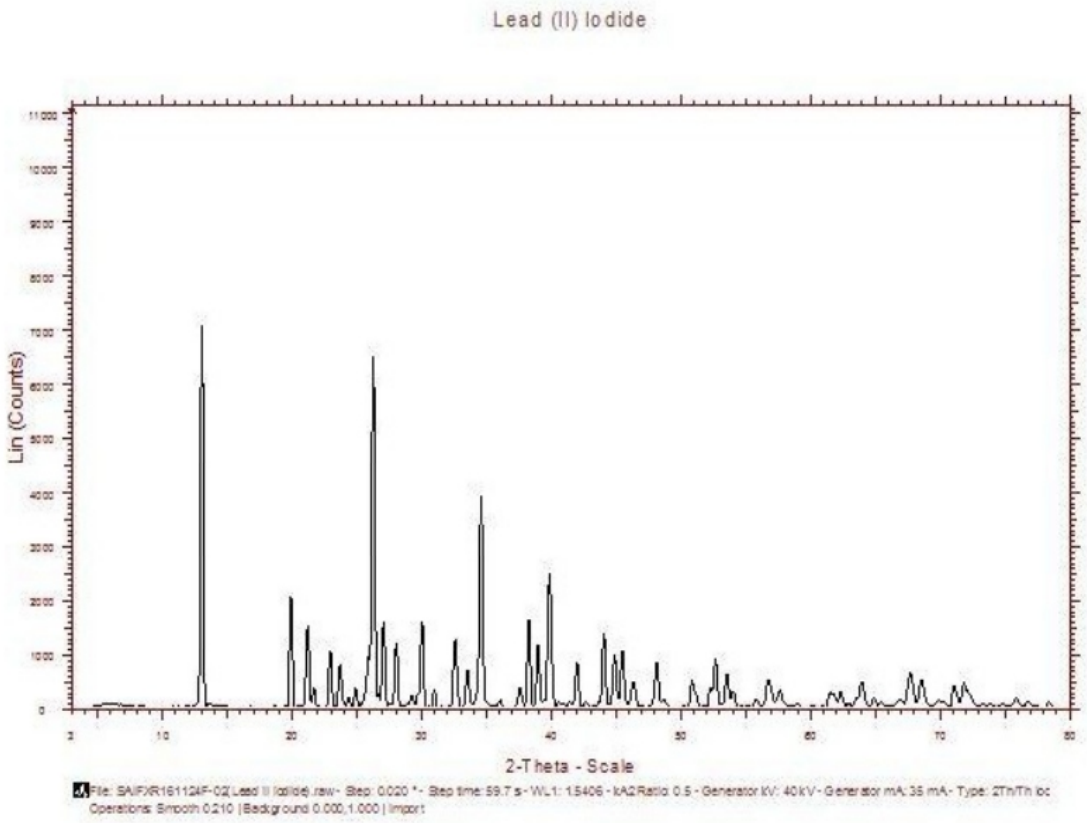

Figure .1. XRD pattern of lead II iodide nanoparticles.

A good agreement between the Experimental diffraction angle [2θ] and Standard diffraction angle [2θ] of specimen is confirming standard of the specimen. Many peaks at 2θ values of Lead iodide is observed and tabulated in table.1 and compared with the standard powder diffraction card of Joint Committee on Powder Diffraction Standards (JCPDS), Lead II iodide file No. 89-1974. The d-spacing values of experimental is also confirming to the standard values.

Experimental		Standard – JCPDS 89-1974	
Diffraction angle (2θ in degrees)	D spacing (Å)	Diffraction angle (2θ in degrees)	D spacing (Å)
12.945	6.833	12.674	6.979
19.063	4.652	19.06	4.653
22.87	3.885	22.791	4.653
24.837	3.582	24.624	3.613
25.492	3.491	25.568	3.481
26.193	3.399	26.278	3.388

28.353	3.145	28.741	3.104
32.538	2.749	32.135	2.783
34.543	2.594	34.829	2.573
35.982	2.494	35.391	2.534
38.611	2.329	38.674	2.326
39.414	2.284	39.519	2.278
41.381	2.18	41.665	2.119
43.273	2.089	43.907	2.06
46.984	1.932	46.96	1.933
47.169	1.925	47.119	1.927
47.578	1.909	47.663	1.906
49.395	1.843	49.593	1.837
52.305	1.747	52.399	1.744
58.571	1.574	58.462	1.577
64.931	1.435	64.732	1.439
66.82	1.398	66.774	1.399
66.929	1.396	66.991	1.395
67.495	1.386	67.569	1.385
73.149	1.293	73.149	1.293
66.929	1.396	66.991	1.395
67.495	1.386	67.569	1.385
73.149	1.293	73.149	1.293

Table.1. Experimental and standard diffraction angles of lead II iodide nanoparticles.

XRD – DISLOCATION DENSITY

The dislocation density is defined as the length of dislocation lines per unit volume of the crystal. In materials science, a dislocation is a crystallographic defect, or irregularity, within a crystal structure. The presence of dislocations strongly influences many of the properties of materials. The movement of a dislocation is impeded by other dislocations present in the sample. Thus, a larger dislocation density implies a larger hardness.

The X-ray line profile analysis has been used to determine the dislocation density.

The dislocation density can be calculated from equation

$$\delta = \frac{1}{D^2}$$

Where δ is dislocation density and D is the crystallite size. Results of the dislocation density calculated from the formula is given in table.2. The number of unit cell is calculated from equation

$$n = \pi\,(4/3) \times (D/2)^3 \times (1/V)$$

Where D is the crystallite size and V is the cell volume of the sample.

2θ (deg)	Particle Size	Dislocation Density	Number of
		$(m^2)\ x10^{15}$	Unit Cell
	D (nm)	$\delta = 1 / D^2$	$X10^5$
12.947	30.79	1.054	3.648
19.826	30.56	1.071	3.568
26.193	29.11	1.18	3.083
34.543	28.08	1.268	2.767
39.824	24.22	1.705	1.796

Table .2. Dislocation Density and Number of Unit Cell from XRD of lead II iodide nanoparticles.

It is observed from these tabulated details, and from figure.2, figure.3 and figure.4, dislocation density is indirectly proportional to particle size and number of unit cells. Dislocation density increases while both particle size and number of unit cell decreases.

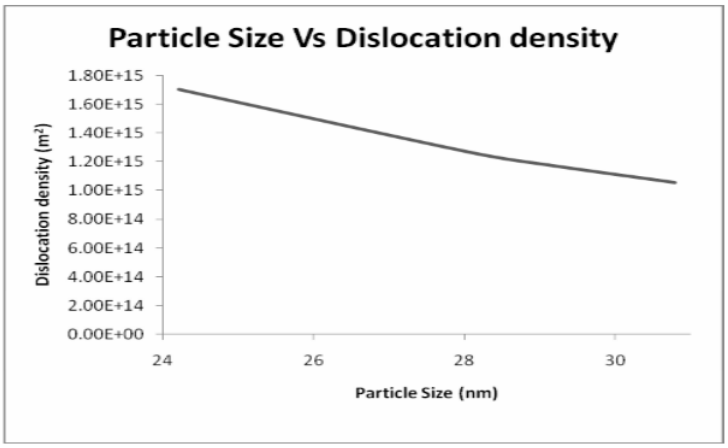

Figure.2. Particle size Vs Dislocation density curve of lead II iodide nanoparticles.

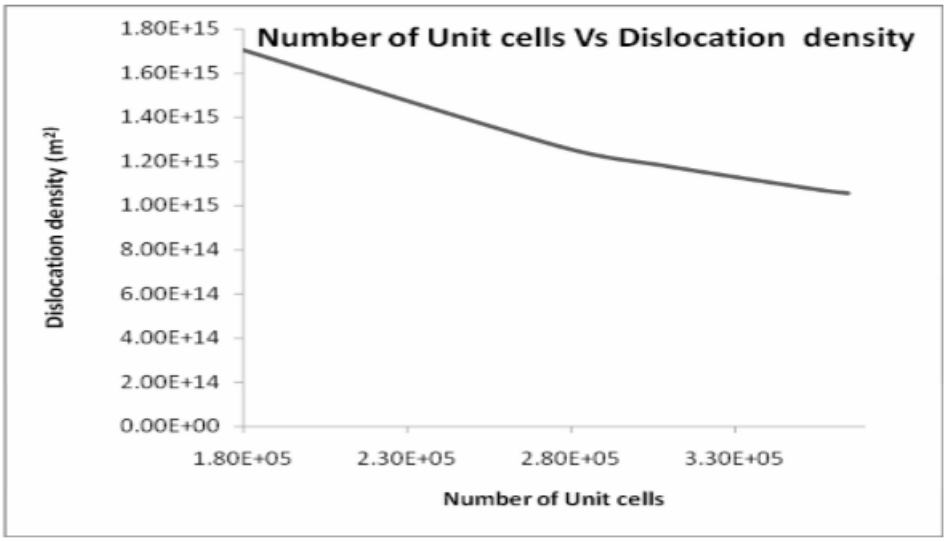

Figure.3. Number of Unit cells Vs Dislocation density curve of lead II iodide nanoparticles.

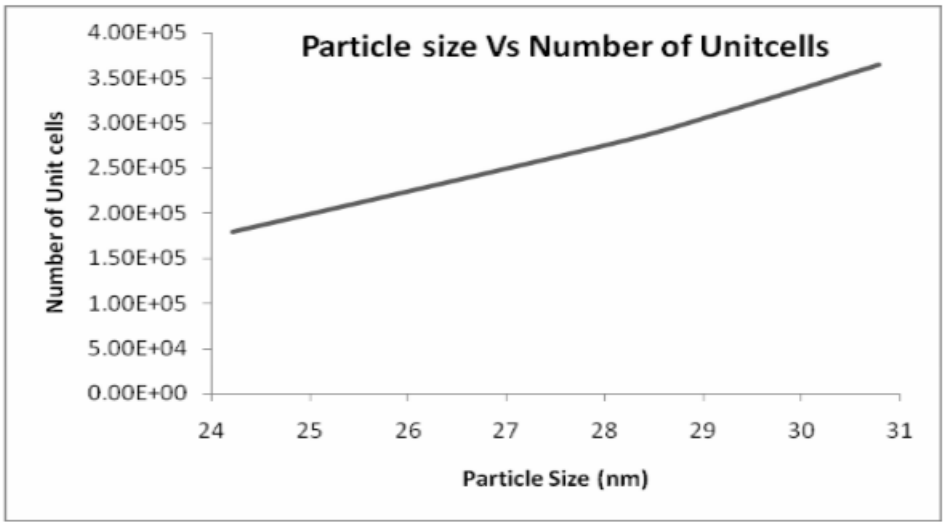

Figure.4. Particle Size Vs Number of Unit cells curve of lead II iodide nanoparticles.

XRD – MORPHOLOGY INDEX

A XRD morphology index (MI) is calculated from FWHM of XRD data using the relation

$$M.I = \frac{FWHM_h}{FWHM_h + FWHM_p}$$

Where M.I. is morphology index, $FWHM_h$ is highest FWHM value obtained from peaks and $FWHM_p$ is value of particular peak's FWHM for which M.I. is to be calculated. The relation between morphology index and particle size is shown in table .3.

FWHM (β) radians	Particle Size(D) nm	Morphology Index (unitless)
0.004506	30.79	0.5
0.004535	30.56	0.4984
0.004268	29.11	0.4362
0.004936	28.08	0.4772
0.005722	24.22	0.4405

Table .3. Relation between Morphology Index and Particle size for lead II iodide nanoparticles.

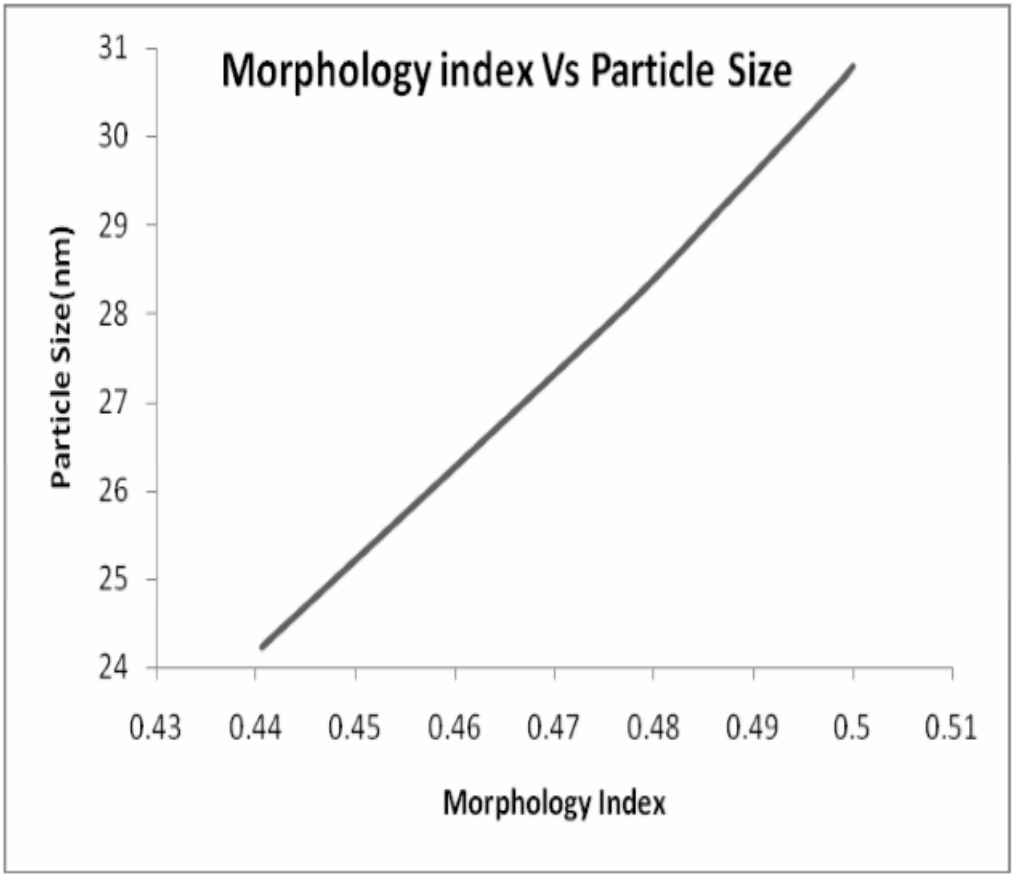

Figure .5. Morphology Index of lead II iodide nanoparticles.

It is observed that MI has direct relationship with particle size and the results are shown in Figure .5.

XRD – UNIT CELL PARAMETERS

Unit cell parameters values calculated from XRD are enumerated in table .4.

Parameters	Values
Structure	Rhombohedral
Space group	R3m (166)
Symmetry of lattice	Rhomb-centered
Particle size	30.8 nm
Lattice parameters	a=4.557;b=---;c=125.62
Vol.unit cell(V)	2259.2
Density (ρ)	6.099
Dislocation Density	$1.054x10^{15}$
Mass	461.01amu

Table .4. XRD parameters of lead II iodide nanoparticles.

SEM STUDIES

Scanning electron microscopy was used to analyze the morphology and size of the synthesized lead II iodide nanoparticles. Figure.6, Figure.7, Figure.8 and Figure.9 show the SEM images of the lead II iodide nanoparticles at various magnifications. The SEM images of lead II iodide nanoparticles show well crystallized particles with spherical shape. In this case the particles sizes are slightly increased and is also observed that the particles are distributed with agglomeration.

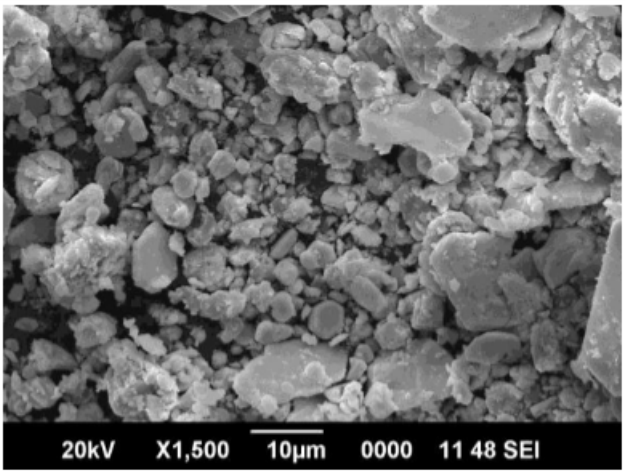

Figure.6. SEM image at 1500 magnifications.

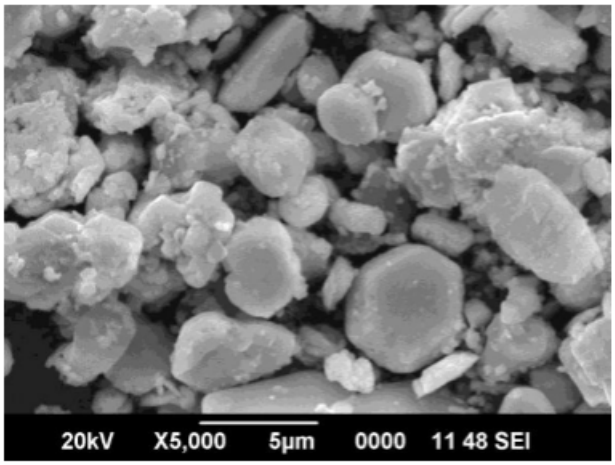

Figure.7. SEM image at 5000 magnifications.

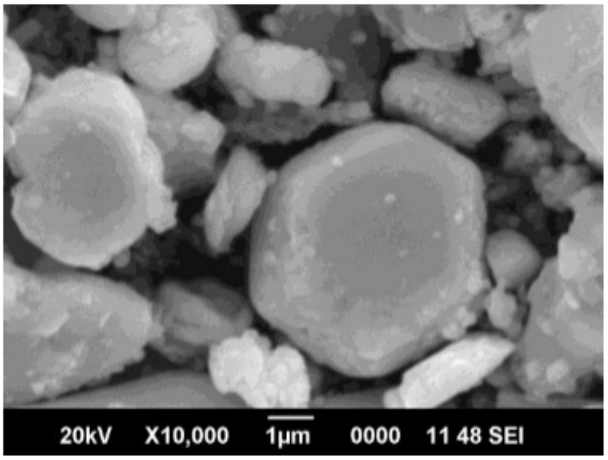

Figure.8. SEM image at 10000 magnifications.

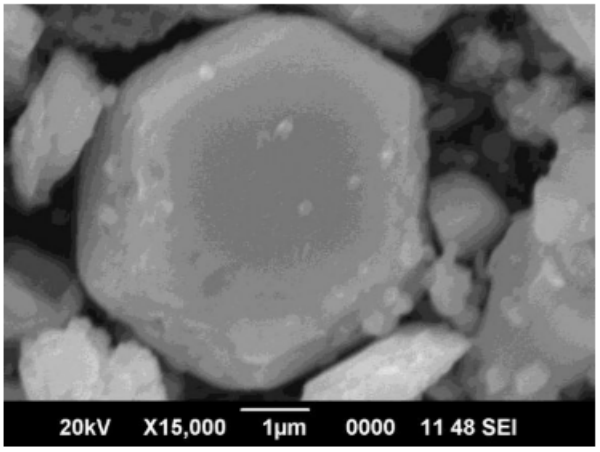

Figure.9. SEM image at 15000 magnifications.

FTIR STUDIES

The FTIR spectrum of the lead II iodide sample is shown in the figure.10.The FTIR spectrum for lead II iodide nanoparticles show peak at 3434.82 corresponds to the free O-H group [3] and the peak at 1159.66 cm^{-1} is due to the presence of lead [4] and the peaks at cm^{-1} and 593.26 cm^{-1} are due to Pb-I bond.

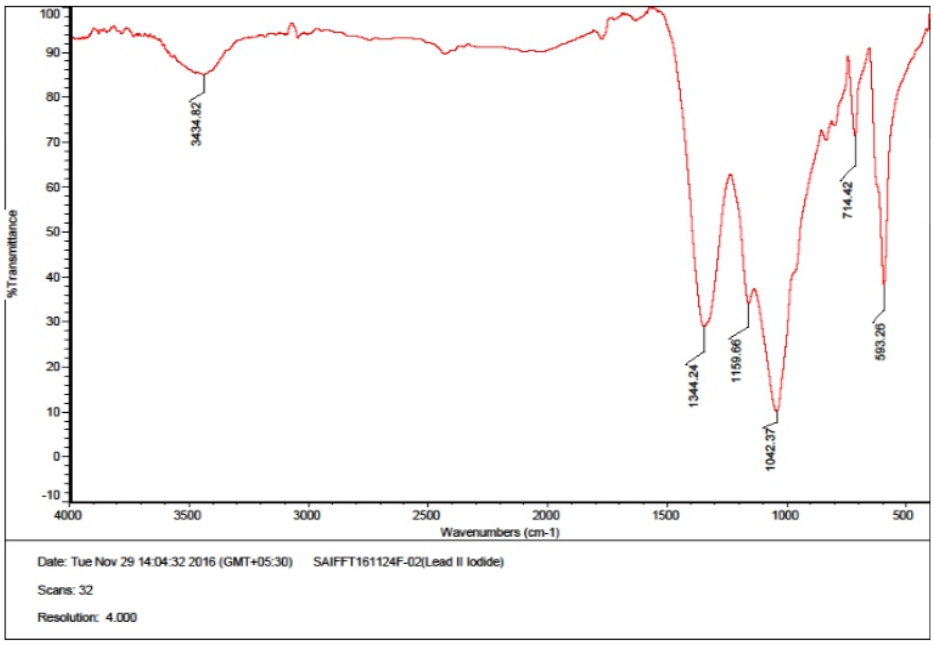

Figure.10. FTIR spectra of lead II iodide nanoparticles.

UV STUDIES

The band gap of the prepared sample lead II iodide was determined by using UV visible studies.. Figure.11 shows the graph to find the band gap of lead II iodide nanoparticles. From the graph, the

optical band gap of lead II iodide is 3.5 eV.

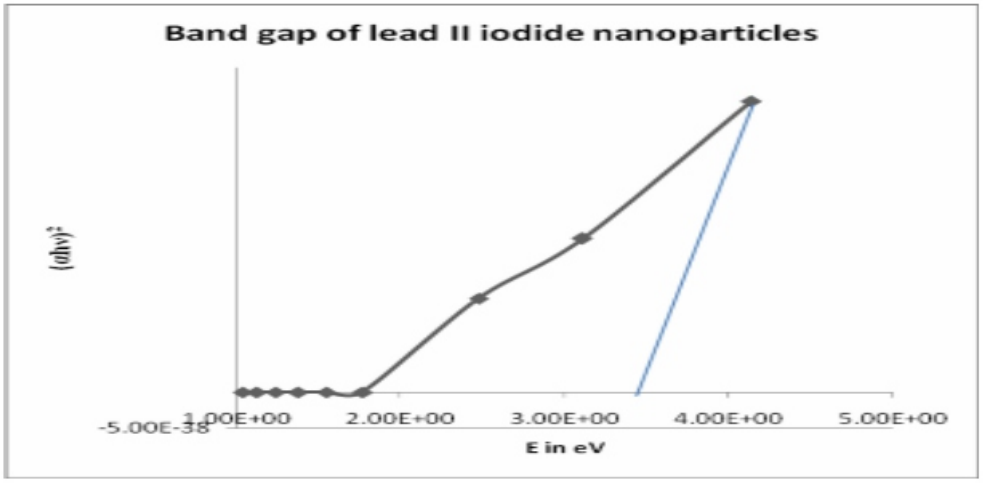

Figure.11. Graph to find the band gap of lead II iodide nanoparticles.

CONCLUSIONS

The **l**ead II iodide nanoparticles have been prepared by chemical co-precipitation method. XRD analysis suggests that the average particle size is in the nano range (30.8nm). The SEM picture reveals the well crystallized particles with spherical morphology. From the FTIR spectrum, the stretching and bending frequencies of the molecular functional groups in the sample are studied. From the UV spectra, the band gap was found.

REFERENCES

1. *Hepzi Pramila Devamani .R and Alagar.M, Synthesis and Characterization of lead (II) phosphate nanoparticles, Elixir Nanotechnology, 61, 2013, 16922 – 16926.*
2. *Alagar.M, Theivasanthi.T, Nano sized copper particles by electrolytic synthesis and characterizations, Int. J. Phy. Sci., 6(15), 2011, 3662-3671.*
3. *Samim.M, Kaushik N.K, Maitra A, Effect of size of copper nanoparticles on its catalytic behaviour in Ullman reaction, Bull. Mater. Sci, 30(5), 2007, 535–540.*
4. *Hepzi Pramila Devamani.R and Alagar M, Synthesis and Characterization of Lead (II) Hydroxide Nanoparticles, Int. J. App. Sci. Eng. Research, 1(3), 2012, 483-487.*

Instructions for Authors

Essentials for Publishing in this Journal

1 Submitted articles should not have been previously published or be currently under consideration for publication elsewhere.

2 Conference papers may only be submitted if the paper has been completely re-written (taken to mean more than 50%) and the author has cleared any necessary permission with the copyright owner if it has been previously copyrighted.

3 All our articles are refereed through a double-blind process.

4 All authors must declare they have read and agreed to the content of the submitted article and must sign a declaration correspond to the originality of the article.

Submission Process

All articles for this journal must be submitted using our online submissions system. http://enrichedpub.com/ . Please use the Submit Your Article link in the Author Service area.

-

Manuscript Guidelines

The instructions to authors about the article preparation for publication in the Manuscripts are submitted online, through the e-Ur (Electronic editing) system, developed by **Enriched Publications Pvt. Ltd**. The article should contain the abstract with keywords, introduction, body, conclusion, references and the summary in English language (without heading and subheading enumeration). The article length should not exceed 16 pages of A4 paper format.

Title

The title should be informative. It is in both Journal's and author's best interest to use terms suitable. For indexing and word search. If there are no such terms in the title, the author is strongly advised to add a subtitle. The title should be given in English as well. The titles precede the abstract and the summary in an appropriate language.

Letterhead Title

The letterhead title is given at a top of each page for easier identification of article copies in an Electronic form in particular. It contains the author's surname and first name initial .article title, journal title and collation (year, volume, and issue, first and last page). The journal and article titles can be given in a shortened form.

Author's Name

Full name(s) of author(s) should be used. It is advisable to give the middle initial. Names are given in their original form.

Contact Details

The postal address or the e-mail address of the author (usually of the first one if there are more Authors) is given in the footnote at the bottom of the first page.

Type of Articles

Classification of articles is a duty of the editorial staff and is of special importance. Referees and the members of the editorial staff, or section editors, can propose a category, but the editor-in-chief has the sole responsibility for their classification. Journal articles are classified as follows:

Scientific articles:

1. Original scientific paper (giving the previously unpublished results of the author's own research based on management methods).

2. Survey paper (giving an original, detailed and critical view of a research problem or an area to which the author has made a contribution visible through his self-citation);

3. Short or preliminary communication (original management paper of full format but of a smaller extent or of a preliminary character);

4. Scientific critique or forum (discussion on a particular scientific topic, based exclusively on management argumentation) and commentaries. Exceptionally, in particular areas, a scientific paper in the Journal can be in a form of a monograph or a critical edition of scientific data (historical, archival, lexicographic, bibliographic, data survey, etc.) which were unknown or hardly accessible for scientific research.

Professional articles:

1. Professional paper (contribution offering experience useful for improvement of professional practice but not necessarily based on scientific methods);
2. Informative contribution (editorial, commentary, etc.);
3. Review (of a book, software, case study, scientific event, etc.)

Language

The article should be in English. The grammar and style of the article should be of good quality. The systematized text should be without abbreviations (except standard ones). All measurements must be in SI units. The sequence of formulae is denoted in Arabic numerals in parentheses on the right-hand side.

Abstract and Summary

An abstract is a concise informative presentation of the article content for fast and accurate Evaluation of its relevance. It is both in the Editorial Office's and the author's best interest for an abstract to contain terms often used for indexing and article search. The abstract describes the purpose of the study and the methods, outlines the findings and state the conclusions. A 100- to 250-Word abstract should be placed between the title and the keywords with the body text to follow. Besides an abstract are advised to have a summary in English, at the end of the article, after the Reference list. The summary should be structured and long up to 1/10 of the article length (it is more extensive than the abstract).

Keywords

Keywords are terms or phrases showing adequately the article content for indexing and search purposes. They should be allocated heaving in mind widely accepted international sources (index, dictionary or thesaurus), such as the Web of Science keyword list for science in general. The higher their usage frequency is the better. Up to 10 keywords immediately follow the abstract and the summary, in respective languages.

Acknowledgements

The name and the number of the project or programmed within which the article was realized is given in a separate note at the bottom of the first page together with the name of the institution which financially supported the project or programmed.

Tables and Illustrations

All the captions should be in the original language as well as in English, together with the texts in illustrations if possible. Tables are typed in the same style as the text and are denoted by numerals at the top. Photographs and drawings, placed appropriately in the text, should be clear, precise and suitable for reproduction. Drawings should be created in Word or Corel.

Citation in the Text

Citation in the text must be uniform. When citing references in the text, use the reference number set in square brackets from the Reference list at the end of the article.

Footnotes

Footnotes are given at the bottom of the page with the text they refer to. They can contain less relevant details, additional explanations or used sources (e.g. scientific material, manuals). They cannot replace the cited literature.
The article should be accompanied with a cover letter with the information about the author(s): surname, middle initial, first name, and citizen personal number, rank, title, e-mail address, and affiliation address, home address including municipality, phone number in the office and at home (or a mobile phone number). The cover letter should state the type of the article and tell which illustrations are original and which are not.

Address of the Editorial Office:

Enriched Publications Pvt. Ltd.
S-9,IInd FLOOR, MLU POCKET,
MANISH ABHINAV PLAZA-II, ABOVE FEDERAL BANK,
PLOT NO-5, SECTOR -5, DWARKA, NEW DELHI, INDIA-110075,
PHONE: - + (91)-(11)-45525005